

Toward a unified view of radiological imaging systems. Part II: Noisy images

Robert F. Wagner

Citation: *Medical Physics* **4**, 279 (1977); doi: 10.1118/1.594362

View online: <http://dx.doi.org/10.1118/1.594362>

View Table of Contents: <http://scitation.aip.org/content/aapm/journal/medphys/4/4?ver=pdfcov>

Published by the American Association of Physicists in Medicine

Articles you may be interested in

[Radiological interpretation 2020: Toward quantitative image assessment](#)

Med. Phys. **34**, 4173 (2007); 10.1118/1.2789501

[A unified view of imaging the elastic properties of tissue](#)

J. Acoust. Soc. Am. **117**, 2705 (2005); 10.1121/1.1880772

[Quantitative stereology and radiologic image analysis. Part II: Transmission \(projection\) radiography](#)

Med. Phys. **9**, 361 (1982); 10.1118/1.595095


[A different ... view ... of attenuation ... Part II](#)

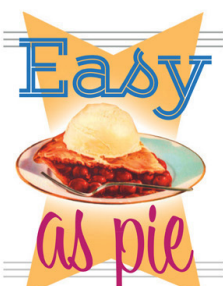
J. Acoust. Soc. Am. **65**, S15 (1979); 10.1121/1.2017131

[Toward a unified view of radiological imaging systems](#)

Med. Phys. **1**, 11 (1974); 10.1118/1.1637272

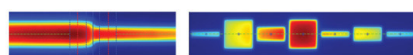
Revised Manuscript to be reviewed





RITG148⁺

Custom Designed
TG-148 Tests
For Tomotherapy QA




RIT is your only source for the tests specified for helical tomotherapy in the TG-148 report. These automated QA tests include:

- Automated QA testing
- Y-jaw divergence/beam centering
- Y-jaw/gantry rotation plane alignment
- Gantry angle consistency
- Treatment field centering
- MLC alignment test
- Couch translation/gantry rotation
- Laser localization
- Image quality tests (Cheese Phantom)
- Built in trending and reporting with RITtrend

These tests are included in both our RITComplete, and RITG148+ products.

Call 719.590.1077,
option 4, or email
mac@radimage.com
today to set up your
personal demo.



©Radimage Technology, Inc., 2016

Toward a unified view of radiological imaging systems.

Part II: Noisy images^{a),b)}

Robert F. Wagner

Medical Physics Branch, Division of Electronic Products, Bureau of Radiological Health, Food and Drug Administration, Rockville, Maryland 20852

(Received 8 September 1976; accepted for publication 3 January 1977)

"The imaging process is fundamentally a sampling process." This philosophy of Otto Schade, utilizing the concepts of sample number and sampling aperture, is applied to a systems analysis of radiographic imaging, including some aspects of vision. It leads to a simple modification of the Rose statistical model; this results in excellent fits to the Blackwell data on the detectability of disks as a function of contrast and size. It gives a straightforward prescription for calculating a signal-to-noise ratio, which is applicable to the detection of low-contrast detail in screen-film imaging, including the effects of magnification. The model lies between the optimistic extreme of the Rose model and the pessimistic extreme of the Morgan model. For high-contrast detail, the rules for the evaluation of noiseless images are recovered.

I. INTRODUCTION

Obviously radiologic imaging has entered a new era: The x-ray-tube focus is being redesigned; color-television technology has supplied more efficient x-ray phosphors; the advance represented by cesium iodide image-tube technology is being refined even further; high-resolution pickup tubes and displays are available; electrostatic detection modalities are succeeding; scatter is being coped with by scanning; and the scanners are being assisted by computers. The possibility now exists for the high-speed acquisition and manipulation of x-ray attenuation information in up to five dimensions (space, time, and energy) and for the realization of the full family of images described by Mistretta.¹

While earlier the quantitative analysis of the acquisition and human utilization of such information in two or more dimensions has been spurred principally by nonmedical applications, an opportunity now presents itself for a shift of the center of gravity of this work into the area of radiology. Indeed, in medicine there is the same set of constraints as in, say, entertainment or defense, viz. to use the available radiation economically for reasons of safety, time, or money; and the same need to rate systems according to this economy and the subsequent efficacy of the display. However, in radiology we have not yet reached a coherent consensus on how to use our measurements on imaging systems and components toward these ends.

We have no lack of data: A recent symposium called by the Bureau of Radiological Health documents the current status of the various measurements.² It is clear that the area of the greatest consensus and refinement in quantification of the radiologic image is the measurement of certain radiographic screen-film characteristics: modulation transfer function (MTF), sensitometric response (D vs $\log E$), Wiener spectrum of system noise (WS), and incident x-ray energy spectrum. These quantities can be measured with a precision (and in some cases, accuracy) on the order of 5%. We believe that someday we will be able to perform a decision theoretic analysis on the radiographic system, carry out some integrals

over the above functions and certain characteristics of the human eye-brain, and predict what can be seen on a radiograph. We expect that we will be able to use these integrals as figures of merit for rating systems, and that the ratings will be dependent on the imaging task. However, at the moment we are not sure how to write down the integrands.

The purpose of this paper is to show that reasonable estimates of system sharpness and meaningful signal-to-noise ratios can be obtained by algebraic means without recourse to cumbersome expressions involving integrals. The hope is that this route will lead us to the physical insight necessary to do a more complete and rigorous analysis using a decision theoretic approach.³ The estimation techniques are based principally on the theory of sample number and sampling aperture of Otto Schade. ("The imaging process is fundamentally a sampling process."⁴) In presenting them, however, we will attempt to construct a synthesis of the views of Rose, Schade, and Shaw, from the nonmedical vantage point, with the available data on medical imaging systems. The data have been derived mainly from the work at the Center for Radiologic Image Research at the University of Chicago (the late Kurt Rossmann directed this work through 1976) and from our own studies here in the laboratories of the Bureau of Radiological Health.

In Secs. II and III we discuss large-area signals, their transfer characteristics, and factors which require renormalization of these characteristics. Sections IV and V deal with some general considerations of noise and basic signal detection. Then in Sec. VI we review the concept of the sampling aperture and its application to the simplification of the problem of image blurring. This is used in Sec. VII to construct the detail signal-to-noise ratio of Schade; in turn, this leads to a straightforward modification of the Rose model, and to excellent fits to the data of Blackwell on visual contrast thresholds.

In Sec. VIII we present a description of how the (apparent) sample number is derived from noise measurements. The concepts of sample number and sampling aperture are combined in Sec. IX to explain the results of experiments in

magnification radiography of noise-limited signals. Finally, in Secs. X–XII some attempts are made toward approaching problem areas from the point of view of the aperture theory.

II. LARGE-AREA SIGNAL TRANSFER CHARACTERISTICS

In radiology, just as in other photographic applications, the large-area signal transfer is characterized by the function which relates the optical density D on the film to the exposure E (here, generally x-ray exposure) to the screen–film system or film alone. The function is usually given in semilog coordinates as the D vs $\log E$ curve. Since density is defined as

$$-D = \log_{10} T, \quad (1)$$

where T is the percent transmission of the film, the D vs $\log E$ curve is really a plot of T vs E in log–log coordinates (suppressing the minus sign). This is an appropriate representation since the intensity (brightness) of light, B , transmitted through the film is proportional to T (the product of T and the intensity of the illuminator). If there is a power-law dependence of T on E , namely $T = E^\gamma$, then this curve will be a straight line with slope γ . Some typical shapes of D , $\log E$ curves in radiology are given in Fig. 1 on the left.⁵ They are obviously not straight lines, indicating a more complicated power dependence. However, their instantaneous slopes, or point gammas $\dot{\gamma}$, have important physical significance. Following Schade,⁴ we define the *incremental-signal transfer factor*

$$g = dT/dE, \quad (2a)$$

and the *large-signal transfer factor*

$$G = \bar{T}/\bar{E}. \quad (2b)$$

(The *small* or *large signals* are both considered to be over *large* areas.) It is readily shown that the *transfer ratio* g/G is equal to the point gamma $\dot{\gamma}$ at the point (\bar{T}, \bar{E}) measured from (0,0):

$$\begin{aligned} \Delta (\log T) &= 0.43 (\Delta T/\bar{T}), \\ \Delta (\log E) &= 0.43 (\Delta E/\bar{E}); \end{aligned}$$

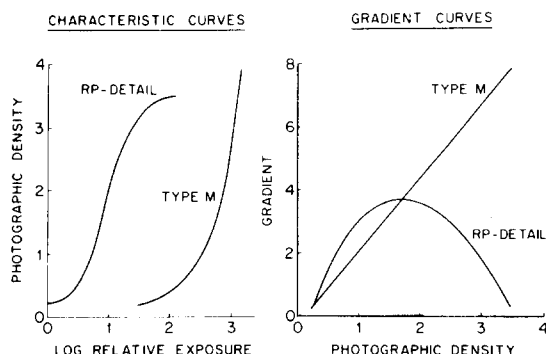


FIG. 1. Large-area transfer characteristics for some typical radiographic systems. Left: D vs $\log E$ for type M film and for RP/Detail film–screen system. Right: gradient curves, or curves of the instantaneous slopes—point gamma—for the same systems (courtesy of K. Doi *et al.* and *Radiology*, Ref. 5).

dividing, we obtain

$$\dot{\gamma} = \frac{\Delta T/\Delta E}{\bar{T}/\bar{E}} = g/G. \quad (3)$$

In this form the expression is useful for analyzing a chain of nonlinear components (as in a TV chain): the point gamma values in the overall transfer characteristic are the product of the respective point gammas of all component characteristics. However, since $\Delta E/\bar{E}$ is the exposure contrast C_{in} and $\Delta T/\bar{T}$ is the brightness contrast C_{out} in the image which is viewed, the point gamma is really a *contrast gain factor*, as is well known:

$$\dot{\gamma} = \frac{\Delta T/\bar{T}}{\Delta E/\bar{E}} = \frac{C_{out}}{C_{in}}. \quad (4)$$

These are simple relationships of fundamental importance in all imaging applications. We shall need them below. For the present, let us make a few interesting observations.

The point gammas for the systems shown in Fig. 1 are given in the right-hand portion of the figure (gradients). In the neighborhood of density 1.0, the point gamma for the screen–film system has a value of about 3.0 (typical for screen–film systems); for the direct-exposure film, the value is about 2. The resulting difference in output contrast is readily visible in radiographs of large-area signals exposed to a density of 1.0 with these systems. However, the point gamma for the direct-exposure film continues to increase with exposure, leading to the possibility of greater contrast with higher exposures and the use of high-intensity illuminators (the latter is required by the greater contrast threshold of the eye at lower light levels—see below).

It is well known that the response of the eye is sublinear ($\gamma < 1$). According to Schade (Fig. 14 of Ref. 6), the point gamma of the response of the cones is about 0.3 at ordinary brightness levels of about 10 ft L. The value *increases* to about 0.4 for levels 1–2 orders of magnitude *lower*, and *decreases* to about 0.2 for levels 1–2 orders of magnitude *higher*. This effect is delicate to use, however, for improving image quality. At the lower light levels, one runs into the requirement of a greater contrast threshold: This can make certain signals undetectable; however, it can also make the noise undetectable, giving a better visual impression in that respect.⁷ And at all levels one must avoid glare (stray, non-image-forming light), which adds a bias level to the eye's operating characteristic, thereby decreasing overall contrast.

An interesting exercise of the chain rule is provided by the above considerations. When a film exposed with screens ($\dot{\gamma} \approx 3$) is viewed under normal conditions ($\dot{\gamma} = 0.3$), the large-area contrast perceived is approximately equal to that contained in the x-ray field: The system of screen–film/eye is almost a linear detector of large-area x-ray contrast!

A useful rule of thumb may be obtained by writing the differential of D vs $\log E$ in the more familiar form

$$\Delta D = \dot{\gamma} \Delta \log E = 0.43 \dot{\gamma} \Delta E/\bar{E}. \quad (5)$$

For systems and conditions where the point gamma takes a value between 2 and 3 (as mentioned in examples above), the

numerical factor in this equation becomes approximately unity. This means that a given fractional change in exposure will result in a density change of about the same numerical value; e.g., an overexposure of about 25% (0.25) will result in a film too dark by about 0.25 optical density (OD) units. This rule is very rough, but frequently quite handy.

III. LARGE-AREA CONTRAST REDUCTION FACTORS

The shape of the large-area transfer characteristic for screen-film systems is basically a function of the *film* itself (as matched to screen light) and its processing. There are at least three factors that mediate between the contrast of the radiation pattern from the patient and this transfer characteristic of the film/processing combination: the screens' own peculiar spectral (energy) response characteristics; the presence of scattered radiation; the presence of off-focus radiation. The first factor can augment or diminish the contrast from the subject; the others diminish it. We now sketch these effects, beginning with the contribution of the screen to contrast.

A. Screen contrast rendition

In Fig. 2 we consider an 80-kVp spectrum incident upon a subject composed of tissue T and bone B. The beam emerging from B is not only more greatly attenuated than the beam from T, it is also spectrally harder. The ideal detector for enhancing this subject contrast is one which has a speed-energy dependence that falls off steeply for harder beams. Certain rare earth screens have the opposite energy

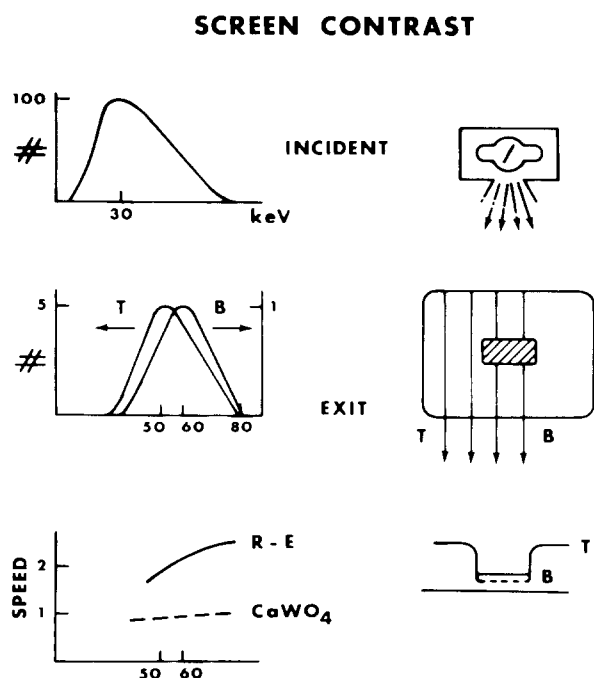


FIG. 2. Schematic representation of the screen (phosphor) contrast rendition factor. The incident x-ray spectrum is not only attenuated more by bone (B) than by tissue (T), it is also hardened more by bone. A screen with a rapidly increasing speed-energy dependence will then diminish subject contrast more than a screen with a more gradual dependence.

TABLE I. Relative screen contrast factor, or intrinsic contrast rendition, for 200- μ screens made from a given phosphor.

| Phosphor | Intrinsic contrast rendition | |
|------------------------------------|------------------------------|-----------|
| | (100 kVp) | (125 kVp) |
| (Zn,Cd)S:Ag | 1.00 | 1.00 |
| Y ₂ O ₂ S:Tb | 0.94 | 0.96 |
| CsI:Na or Tl | 0.85 | 0.86 |
| BaFCl:Eu ²⁺ | 0.83 | 0.80 |
| CaWO ₄ | 0.82 | 0.80 |
| Gd ₂ O ₂ S | 0.71 | 0.72 |

Screen thickness: 200 μ
Filter: 5 mm Al + 150 mm H₂O
Refs. 9 and 10

dependence over a significant portion of the diagnostic energy range.⁸ We might expect them to diminish effective subject contrast compared, say, to calcium tungstate screens. So far, very little quantification of this effect has been carried out. Some calculations have been made of a quantity referred to as the intrinsic screen contrast or contrast rendition factor of a phosphor. This is the input contrast after detection by the phosphor. In the calculation, the contrast differences between 1 mm bone and 1 mm water and between 1 mm water and 1 mm air are averaged; the calculation is based on a 100- or 125-kVp beam with 5 mm Al and 150 mm H₂O added filtration. Results for 200- μ screens are given on a relative scale in Table I.^{9,10} The 10% difference between tungstate screens and gadolinium screens has been difficult to observe in practice, and may be cancelled in part by the fact that the rare earth materials are able to discriminate somewhat against the softer scattered radiation present (following the above argument in reverse).¹¹

These effects have complicated the task of the American National Standards Institute (ANSI) subcommittee PH2.31, which is to arrive at a consensus measurement method for the sensitometry of screen-film processing combinations.^{12,13} Perhaps it will be necessary to specify a *family* of $D, \log E$ curves, or to agree on a phantom, or set of phantoms, for contrast specification. The idea is shown schematically in Fig. 3: Since, over the mid-diagnostic energy range, the $D, \log E$ curve shifts to the left with increasing half-value layer (HVL) of the beam, the effective contrast of materials which attenuate the beam differently (and therefore harden it differently) is lower than that predicted from a single $D, \log E$ curve. One might expect this phenomenon to be significant in a comparison of direct x-ray film and screen-film systems for mammography. Because of the presence of the silver K -absorption edge at 25.5 keV, slight increases in beam HVL (due, say, to transmission through calcium in the breast) will show up as significant increases in direct x-ray film speed compared, say, to screen-film. This should diminish effective subject contrast. (Preliminary measurements indicate that this may be as much as a 25% effect for 500 μ of calcium phosphate in a breast phantom. There is effectively no cancellation of this effect due to scatter rejection: At the low kilovoltage of mammography, the scatter spectrum has essentially the same shape as the primary spectrum.¹⁴)

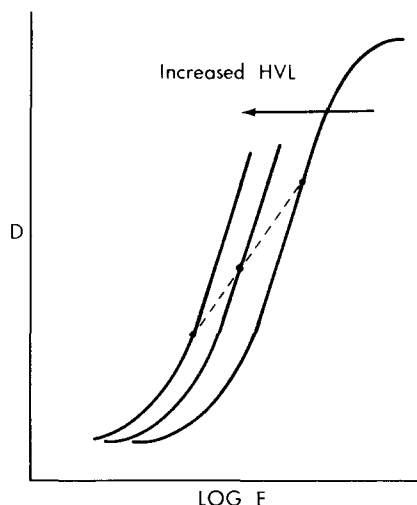


FIG. 3. An equivalent way of looking at the effect sketched in Fig. 2: speed increases (more typically) with increasing HVL. Overall contrast depends on the rate of increase. The dashed line connects $(D, \log E)$ points that result from exposing an aluminum step wedge (differing amounts of hardening) with scatter eliminated.

B. Scattered radiation

The success of the computerized scanners has generated a renewed interest in the problem of scattered radiation, its effect on image quality, and suggestions for its cleanup through the use of ganged scanning slits.^{15,16} Since the literature on this subject is expanding rapidly, we will simply give a few highlights here. In Fig. 4 we give scatter-to-primary ratios (S/P) as measured by Gould¹⁷ (modified by Shuping¹⁸) as a function of field size for a number of thicknesses of Pressdboard phantom (the method of Ref. 19 was used). The data follow the same trends observed elsewhere^{20,21} and indicate that for situations approximating examinations of large body sections using large field sizes, values of S/P ranging from about 5 to 10 might be expected. For low radiation contrast, and a situation where the scatter is uniform over signal and background areas, the primary contrast $\Delta P/P$ will be reduced to $\Delta P/(P + S)$: The primary

contrast is reduced by a factor $(1 + S/P)^{-1}$. [If we compare a scatter-free situation with a situation with scatter present, and expose to the same number of *primary* counts, scatter then degrades the signal-to-noise ratio by a factor $(1 + S/P)^{-1/2}$. An analysis of the efficiency of utilization of the information in the radiation stream for a number of interesting cases of scatter plus cleanup is given by the author in Ref. 22.] In the example just given this means that only about 10%–15% of the primary contrast is realized in the presence of scatter. Even when grids are used, the scatter remaining may be on the same order as the primary for a situation with an initially high value of S/P .^{15,20} This leaves significant latitude for improvement, as several investigators have noted.^{15,16}

C. Off-focus radiation

The presence of off-focus radiation from x-ray tubes produces a reduction in contrast analogous to that produced by scatter. The contrast reduction factor has the same form as that just given, where the ratio S/P is replaced by the ratio of off-focus to on-focus radiation. (A more exact treatment would have to consider directional effects—see Fig. 5—and geometry.) Values of this fraction as high as 1/3 have been observed.^{23,24} This results in a contrast reduction factor on the order of 0.75. (Flare in optical components and veiling glare in image tubes can be handled in a similar fashion to first order, since they are generally large-area effects.) Most of this off-focus radiation could be eliminated through the use of collimating fingers within the tube housing.

IV. NOISE CONTRAST

Up to this point we have neglected the granular nature of the radiation impinging on the detectors we are trying to characterize. However, for image detectors using radiation with wavelengths of roughly 10μ or smaller, including the human eye, it is this granular nature that imposes the fundamental limitation on the quality and detectability of the image.^{7,25,26} Also, in this end of the spectrum it can be assumed that the distribution of quanta in a “uniform expo-

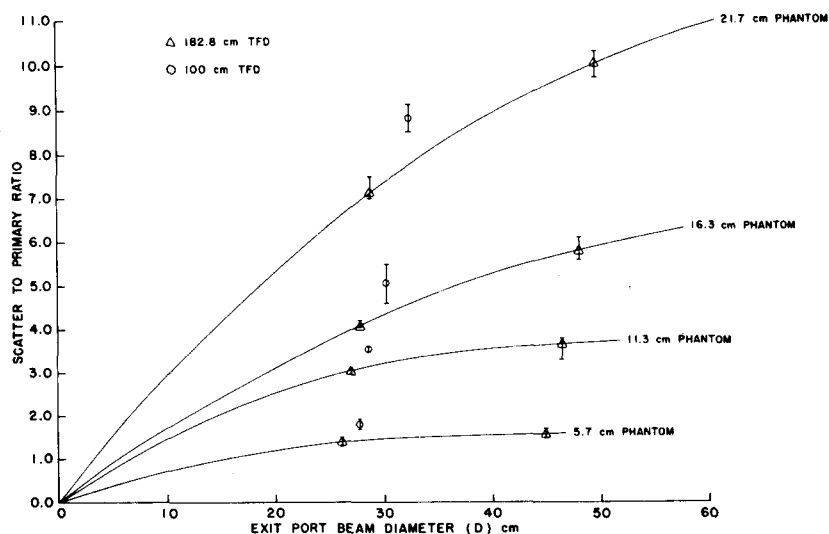


FIG. 4. Measurements of the scatter-to-primary ratio (S/P) exiting from various thicknesses of Pressdboard phantoms (shown as curve parameter) radiated with diagnostic quality x-ray beams, as a function of field size (Refs. 17, 18).

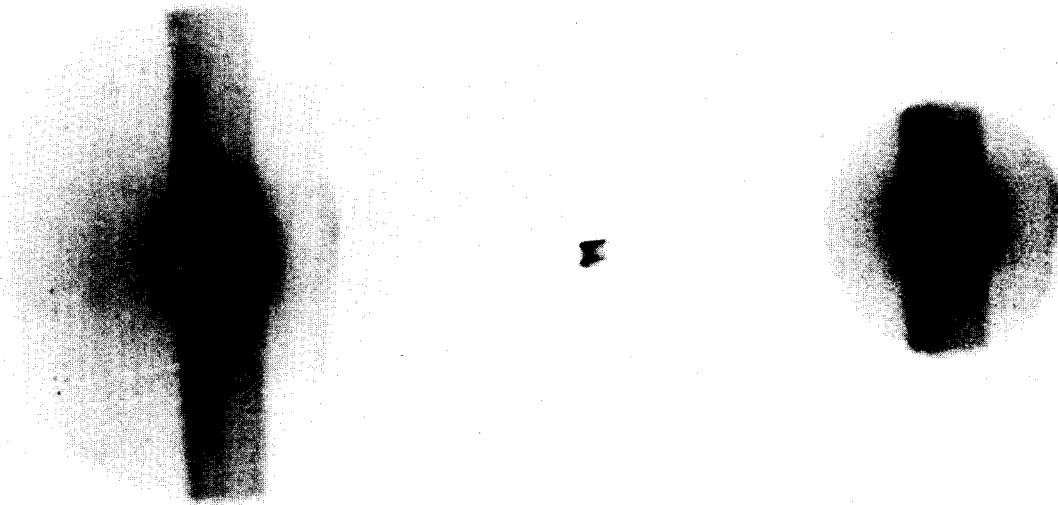


FIG. 5. Pin-hole radiographs of (left) undiaphragmed off-focus radiation, (center) focal spot, and (right) off-focus radiation in which the beam has been diaphragmed at the tube port to allow a maximum field diameter of 17 in. at a distance of 40 in. (to same scale) (Ref. 24).

sure" follows Poisson statistics; i.e., if the average number of quanta falling on a unit area has the value N (number/area), then the root-mean-square (rms) deviation or standard deviation characterizing the fluctuation of this number is given by $N^{1/2}$. With this distribution the number of quanta falling in a given area is uncorrelated with the number falling in any other area. A spatial frequency analysis would then show that no spatial frequency is favored over another—all are equally likely, i.e., the noise has a "white" spectrum. Then the average number falling in *any* area a is equal to Na and the standard deviation of this number is $(Na)^{1/2}$. We will call the area a the *sampling area*, and can define a signal-to-noise ratio based on the background (no signal) Na and the rms noise $(Na)^{1/2}$ as

$$\text{SNR}_a = Na / (Na)^{1/2} = (Na)^{1/2}. \quad (6)$$

Schade calls this the signal-to-noise ratio for the sampling aperture a , for the gray-scale level determined by N .²⁷ We may also think of this, however, as the inverse of a noise contrast⁶ for the area a . This follows by analogy with, say, exposure contrast—the ratio of a difference signal ΔE to the background E . Here we can write

$$C_{\text{noise}} = (Na)^{1/2} / Na = (Na)^{-1/2}, \quad (7)$$

the ratio of the rms noise "difference" to the background. Note that the larger the sampling area, the smaller the noise contrast. The reader who finds this unintuitive may take it as a definition for the moment.

If the noise contrast in a beam with flux density N is now considered as input to a nonlinear system with a point gamma at this operating level of $\dot{\gamma}$, the output noise contrast becomes

$$C_{\text{noise out}} = \dot{\gamma}(Na)^{-1/2}. \quad (8)$$

For example, consider a screen-film system exposed to a density in the neighborhood of 1.0. We will see below that this

requires use of $(3-6) \times 10^4$ x-ray quanta/mm², say 4. The noise contrast at the input to the detector characteristic is then 0.5% in a sampling area of 1 mm². This receives an amplification of $\dot{\gamma} = 3$ and the noise contrast for this size area on the film becomes approximately 1.5%. According to the observations of Schade^{6,28} the eye can see noise contrast of less than 1% in an unmodulated field at a high light level; this threshold goes up to a few percent when the field is modulated by an image structure which can mask the noise. These observations are in general agreement with the observations of viewers of radiographs; the "quantum mottle" is quite in evidence in smooth fields under ordinary viewing conditions, but is easily masked by the structure of an image. If a radiograph is made with a normal exposure but is underdeveloped by hand processing to a gamma of about 1.5, the mottle is only visible after very close inspection. (This analysis involves introducing the sampling aperture of the eye, which is done below. The sampling of 1 mm² here is not unreasonable for an unsharp screen and normal viewing conditions.)

V. SIGNAL DETECTION

One of the motivations for the definitions of signal and noise contrast given above is found in the theory of signal detection. In its barest essentials this theory reduces to a treatment which is commonly referred to as the "Rose model," after Albert Rose who showed the suitability of a statistical analysis for a large class of detectors, including the eye.²⁵ In this model the *area of the object to be imaged is taken as the sampling area for noise* (Rose referred this area to the retina, since he was analyzing visual threshold detection). Then the smallest signal difference that can be detected is proportional to the rms fluctuations in the background (same sampling area) according to the relation

$$\Delta(Na) = k(Na)^{1/2}. \quad (9)$$

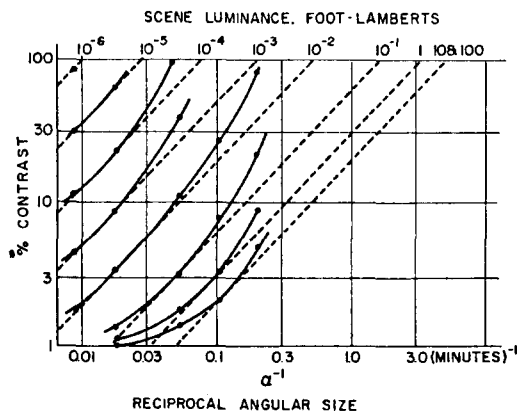


FIG. 6. Visual performance data as measured by Blackwell (Ref. 29)—points joined by solid curve. Visual performance according to Rose model [Eq. (11)] of noise limitation—dashed lines (courtesy of A. Rose and Plenum Press; see Refs. 7, 25).

ΔN is the signal difference in the flux; $\Delta(Na)$ is the difference in total counts. This relation can be written

$$\frac{\Delta N/N}{(Na)^{-1/2}} = k, \text{ for "detection,"}$$

$$C_T(Na)^{1/2} = k. \quad (10)$$

This is one motivation for the definitions of contrast commonly used and given above: The ratio of the input signal contrast, $C_T = \Delta N/N$, to the noise contrast $(Na)^{-1/2}$ must be equal to some value k for detection at some level of probability. This level is usually taken to be 50% and k , the threshold SNR, is usually found to take on a value between 2 and 5. (Some derivations absorb a factor $2^{1/2}$ into k —as implicitly done here. This factor comes about from the fact that both the signal and the background levels are noisy, and the variance of the signal difference is the sum of the variances of each level.)

In treating the human eye, Rose rewrote Eq. (10) as

$$BC_T^2 \alpha^2 = \text{constant},$$

$$C_T = k(1/\alpha), \quad (11)$$

where B , the scene luminance, is proportional to the background flux N , and α is the angle subtended at the lens of the detector (eye) by the signal object, whose linear dimension is proportional to $a^{1/2}$. Rose replotted the data of Blackwell²⁹ on the threshold contrast required to detect gray disks on a white background, as a function of reciprocal angular size of the disk, with scene luminance as a parameter. Rose's figure is reproduced as Fig. 6. If the data followed the model summarized in Eq. (11), they would fall on 45-deg lines as shown. (These are drawn tangent to the best performance at each value of scene luminance.) Rose concluded, "the degree of fit is . . . sufficiently good for many engineering purposes . . . also . . . to draw significant conclusions regarding the mechanism of the eye."²⁵ The principal conclusion was that the performance of the eye approaches that of an ideal picture pickup device, "that is, one limited only by random fluctuations in the primary photo process." This conclusion was of considerable importance in simplifying the analysis of problems involving comparisons of the performance of the eye and man-made devices and confirmed the suitability of

using the concept of (detective) quantum efficiency for making this comparison. (See Ref. 22 for some applications of this concept to radiology.)

Besides the motivation for the definition of contrast just given, we recall in Sec. II the ease of treatment of such a quantity when it is transferred through a nonlinear characteristic. A psychophysical factor that requires such a definition for contrast is the fact that the eye response is sublinear ($\gamma < 1$). Equal increments in counts, exposure quanta, or whatever measure of light intensity are not responded to equally by the human eye. This requires a renormalization of such increments by some power of the background level. The fact that the eye response (as in the case of other senses) is often approximated by a logarithmic function gives added utility to such definitions as $\Delta N/N$, $\Delta I/I$, $\Delta E/E$, etc.

There is further motivation from the point of view of the physics of the radiographic (or photographic) process. A definition of contrast in one of the equivalent forms just given, $\Delta N/N$ say, makes contrast a fundamental property of the material being imaged, independent of exposure level. For example, if we wish to image a lesion of length x (in the direction of the radiation beam) which differs in linear attenuation coefficient from neighboring tissue material by an amount $\Delta\mu$, then the quantities $\Delta N/N$ or $\Delta E/E$ on the downstream side are given approximately by

$$\Delta N/N \approx \Delta\mu x, \quad (12)$$

for $\Delta\mu x$ small compared to unity.

This point provides an opportunity to clear up some confusion in the literature on computer-assisted tomography (CT). It is generally recognized that, at common photon counting levels³⁰ (about 10^5 /transmission measurement, and pixels 1.5 mm square), a lesion that differs in linear attenuation coefficient by 1% from that for water ($\mu_{H_2O} \approx 0.190 \text{ cm}^{-1}$ at typical operating technique) can be detected if it is large enough, say 1 cm. This value of 1% has been used to deduce that a number on the order of 10^4 counts/measurement is required and one suspects that the scanners may be somewhat inefficient. However, from the above definition of contrast, we see that such a lesion represents a radiation contrast of 0.002 or 0.2% ($\Delta\mu = 0.002 \text{ cm}^{-1}$, $x = 1 \text{ cm}$, $\Delta\mu x = 0.002$)! A very rough calculation of the SNR for this example (1-cm lesion, say 10^2 mm^2) follows:

$$\text{SNR} = C(Na)^{1/2} \stackrel{\text{must}}{=} 2-5, \text{ for detection}$$

$$= 2 \times 10^{-3} \left(\frac{10^5}{1.5 \times 1.5 \text{ mm}^2} \times 10^2 \text{ mm}^2 \right)^{1/2} \approx 4.$$

Using our definition of radiation contrast we see that the other parameters are consistent. The flux density used here is approximately the same as that in general purpose radiography. Such a lesion could therefore be detected conventionally were it not for the degradation due to scatter, the averaging out of contrast by variations in the overlapping structures, and the threshold of the eye. (Here we have neglected the correlation of the noise—see Ref. 22 for further discussion.) By substituting Eq. (12) into Eq. (10), as we have done here, we are essentially deriving a "Rose model for ra-

diography": For a spherical or cubical signal structure, the flux requirements for a given SNR go as the inverse fourth power of the linear dimension; for a prism or cylindrical structure, the flux requirements go as the inverse third (CT) or inverse second power of the linear dimension, depending on the projection and scaling of the structure.

VI. DETAIL CONTRAST: THE CONCEPT OF THE SAMPLING APERTURE

In the section on large-area contrast (Sec. III) we neglected the transition region (edge) between areas of different exposures; in the section on noise contrast (Sec. IV) we neglected to ask how the uncorrelated input quanta are imaged. In reality, any imaging device spreads out sharp edges, images points as blurs, and thereby also introduces correlation among noise samples. For example, a scanning microdensitometer with a large sampling aperture degrades a sharp edge, images points into a blur having the shape of the aperture (neglecting optical effects), and introduces correlations among grains that fill the aperture. Following Schade,³¹ we will call this effect the sampling aperture effect. More complicated blur functions [point spread function (PSF), or apertures with nonuniform transmission] can be reduced to equivalent apertures of uniform transmission by methods introduced by Schade. They are based on the concept of the noise-equivalent passband N_e , defined as the integral of the squared modulation transfer function (MTF):

$$N_e = \int_{-\infty}^{\infty} \text{MTF}^2(f) df. \quad (13)$$

N_e has the dimension of inverse length, and is generally quoted as (TV) lines/length, where the number of lines divided by 2 equals the corresponding frequency f_e . Systems with identical values of N_e are equivalent in the following sense: If noise with a white spectrum is input to the system, they pass the same noise power as a system with an MTF which is unity within the passband and zero outside. [For the case of the one-dimensional passband, this is only strictly true for noise which has structure in only one dimension (see Ref. 31).]

A two-dimensional passband can be defined as in Part I³² of this series³³:

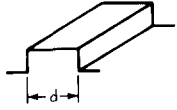
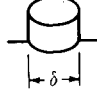
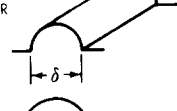
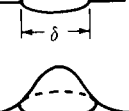
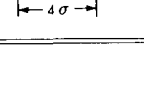
$$N_e^{(2)} = \int \text{MTF}^2(f_x, f_y) df_x df_y, \quad (14)$$

which has the dimension of inverse area. Although defined in terms of noise, N_e was shown by Schade³⁴ to be a measure that correlates well with the general subjective impression of image sharpness in both television and photographic images. Its utility in this connection has been documented many times by Schade and others but perhaps most dramatically in the photographs in Schade's recent book.²⁸ This measure has wide applicability, as we shall review below.

If one already knows the line spread function (LSF) or point spread function (PSF) of an aperture function, it is generally trivial to calculate N_e using Parseval's theorem for the integrated intensity of these functions:

$$N_e = \frac{\int \text{LSF}^2(x) dx}{[\int \text{LSF}(x) dx]^2} \quad (15)$$

TABLE II. Some commonly encountered aperture functions, their one- and two-dimensional passbands and equivalent widths or diameters.

| APERTURE | N_e | Equivalent Width In 1-D Case | $N_e^{(2)}$ | Equivalent Diameter In 2-D Case |
|---|-----------------------|------------------------------|---------------------------|---------------------------------|
| EXPONENTIAL MTF e^{-df} | $\frac{1}{d}$ | d | $\frac{\pi}{2d^2}$ | $0.9d$ |
| SLIT  | $\frac{1}{d}$ | d | | |
| PILL BOX  | $\frac{1.08}{\delta}$ | 0.93δ | $\frac{4}{\pi\delta^2}$ | δ |
| (HALF) CYLINDER  | $\frac{1.08}{\delta}$ | 0.93δ | | |
| (HEMI) SPHERE BEAD  | | | $\frac{9}{32\pi\delta^2}$ | 0.94δ |
| GAUSSIAN PSF  | | | $\frac{1}{4\pi\sigma^2}$ | 4σ |

and

$$N_e^{(2)} = \frac{\int \text{PSF}^2(x, y) dx dy}{[\int \text{PSF}(x, y) dx dy]^2}. \quad (16)$$

If we are dealing with apertures having uniform transmission (as in the case of a microdensitometer aperture where the optics introduce negligible degradation), then these expressions give the immediate result that in one dimension (two dimensions) the passband is the reciprocal of the aperture width (area). In Table II we present some useful aperture functions together with the length d , or diameter δ , of a uniform aperture with the same equivalent passband. These will allow us to solve algebraically some important problems of blurring (convolution). But first some observations. Most likely if we had guessed the equivalent aperture sizes we would have come within 10%. This is quite satisfying to the pedagogical or engineering spirit that likes to be equipped to do calculations on a desert isle. Note that the LSF corresponding to a pill box PSF has the profile of a cylinder. Finally, the equivalent diameter for a Gaussian PSF is proportional to the standard deviation σ of the Gaussian distribution. This leads one to consider an important approximation.

When a Gaussian PSF is blurred (convolved) with another Gaussian PSF, or with a Gaussian object distribution, the result is also Gaussian and has a standard deviation related to that of the first two by triangular addition. It has been found that using the same rule for apertures that are not Gaussian generally leads to very good approximate results, especially as more and more elements are cascaded together:

$$d_{\text{system}}^2 = d_1^2 + d_2^2 + \dots + d_n^2, \quad (17)$$

DETAIL BLURRING (CONVOLUTION)

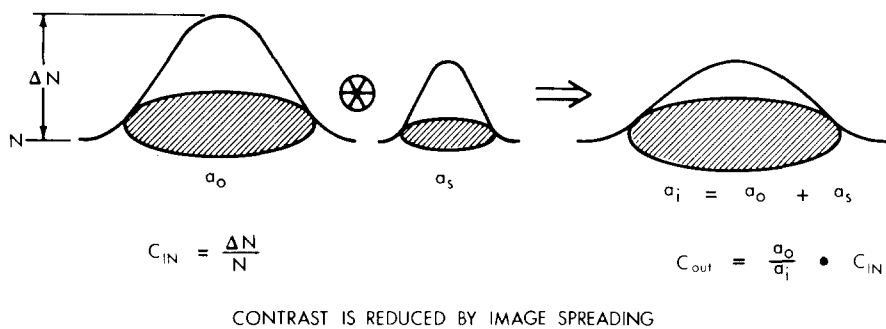


FIG. 7. Schematic representation of the reduction of detail contrast by image spreading (blurring or convolution).

or, in terms of the area a of the apertures,

$$a_{\text{system}} = a_1 + a_2 + \dots + a_n. \quad (18)$$

If an object with an equivalent sampling area a_o is blurred by a PSF with an equivalent sampling area a_s , the sampling area a_i of the resulting image is then simply

$$a_i = a_o + a_s. \quad (19)$$

Again, if the sampling distributions were exactly Gaussian, then the contrast in the image distribution, C_i , would be related exactly to the contrast in the original object distribution, C_o , by the contrast reduction factor (CRF):

$$\text{CRF} = a_o/(a_o + a_s) = a_o/a_i, \quad (20)$$

i.e.,

$$C_i = C_o(a_o/a_i). \quad (21)$$

This is shown schematically in Fig. 7. These relations will be used as approximations when the distributions are not Gaussian.

An example of the application of these approximations to a case where neither distribution is Gaussian can be taken from the work of Haus and Rossmann^{35,36} on blood-vessel imaging. Images of a 0.5-mm-diameter blood-vessel phantom were made on direct-exposure x-ray film, and on screen-film using three different sets of intensifying screens: Radelin TF-2, DuPont Par, and DuPont Detail screens. The images were scanned with a microdensitometer and the resulting density traces were converted to relative exposure profiles using the sensitometric response curves of the image receptors. The final results are reproduced in Fig. 8. (The input

pattern is from the trace of the image made on direct x-ray film, which introduces essentially no degradation when imaging a 0.5-mm object.) The unsharpness introduced by the screens can be seen from the spreading out of the edge of the image and the overall reduction in contrast. The latter can be calculated approximately using the aperture techniques given above.

First the cylindrical object input is considered as a sampling aperture. An exact treatment of this problem must consider the exponential attenuation through the contrast medium. Let us consider two extremes. If the attenuation of the contrast medium is very small, the profile of the attenuated beam is proportional to the profile of a cylinder (first-order Taylor term). The proportionality constant determines the input contrast to the image receptor but it does not determine the sampling aperture size of the object. [The constant cancels out in Eq. (15)]. In this case, the one-dimensional sampling aperture for the blood vessel as found from Table II is 0.93 times the vessel diameter. If the attenuation of the contrast medium is very great, the profile of the attenuated beam is proportional to the profile of a slit (i.e., the center will attenuate hardly more than the periphery). In this case the sampling aperture approaches the diameter of the blood vessel. Particular cases fall between the two extremes just considered. Here we will use the factor 0.93, thus introducing a small error.

The sampling apertures for the screens are taken from exponential fits to their MTFs as discussed in Part I. The values of the exponent d (therefore, the one-dimensional sampling width—see Table II) determined according to the references of Part I³⁷ are given in Table III. The sampling

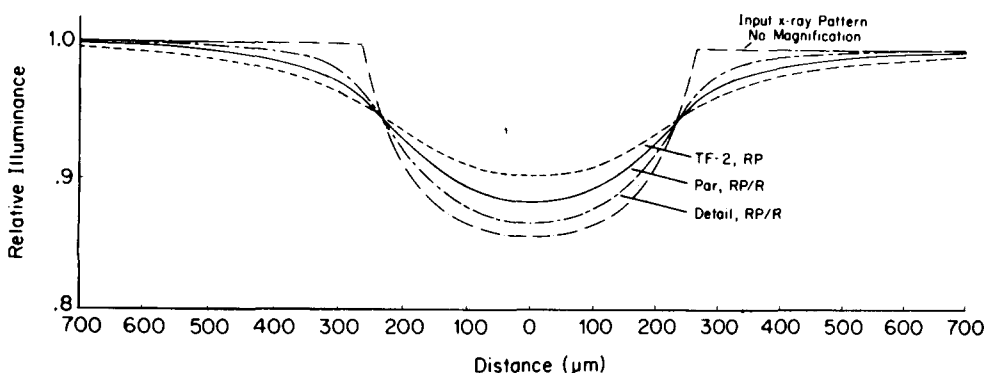


FIG. 8. Input x-ray pattern of a 0.5-mm-diameter blood-vessel phantom and corresponding outputs or relative illuminance distributions in the emulsion using several screen-film systems, showing image blurring due to fluorescent screens (courtesy of A. Haus and K. Rossmann and C. V. Mosby Co.; see Refs. 35, 36).

TABLE III. One-dimensional sampling apertures (widths) for blood vessel and screens of Fig. 8, together with one-dimensional contrast reduction factors from Fig. 8 and from aperture theory.

| Blood vessel example | | |
|---------------------------|--|--|
| Vessel | $d_{\text{low contrast}} = 0.47 \text{ mm}$ | |
| | $d_{\text{high contrast}} = 0.50 \text{ mm}$ | |
| Screens | Detail $d = 0.22 \text{ mm}$ | |
| | Par $d = 0.42 \text{ mm}$ | |
| | TF-2 $d = 0.72 \text{ mm}$ | |
| Contrast reduction factor | | |
| From figure | From aperture theory | |
| Detail 0.93 | 0.90-0.92 | |
| Par 0.80 | 0.75-0.77 | |
| TF-2 0.67 | 0.54-0.57 | |

widths of the blood vessel and the screens are now combined according to the triangle rule of Eq. (17). Since the blood-vessel image is only degraded in one dimension, the CRF becomes d_o/d_i , the ratio of the object to image sampling widths. In Table III we give the values of the CRF as determined from Fig. 8 and as calculated in the manner just described.

The agreement is excellent except for the last case. There are many sources of small errors in an exercise of this kind (including considerations of attenuation, scatter, and using a published figure as an intermediary). If the value of d is an overestimate (especially in the case of TF-2 screens), the indications are that this might be a very good approach for estimating contrast reduction from a single parameter, if it is available. A program has been initiated in our laboratories to collect MTF data and calculate imaging parameters such as the sampling aperture. If the results of further studies exceed the expectations indicated here (i.e., better than 10% agreement), they will be published in handbook form for users of general radiographic systems.

The author and colleagues have applied the aperture theory to magnification radiography³² and to an interesting example of limitations on sharpness imposed by motion and tube loading considerations.²⁴ In these cases the object aperture was neglected; the results reduce to one of the rules of classical unsharpness analysis. Since both of these sets of examples included the x-ray-tube focal spot, it would seem instructive to include a similar example here for completeness. The example chosen is a "Monday morning" analysis of the long-cone, intensifying-screen technique suggested by Haus and colleagues for low-dose mammography.³⁸ These investigators designed a long cone and corresponding configuration to be used with their Senographe (CGR) tube when doing low-dosage mammography using the (DuPont) Lo-Dose screen-film system, and compared the resulting system MTFs and images with those obtained using the original short-cone technique and RP/M (Kodak) direct x-ray film. The before and after geometries are reproduced in Fig. 9, including the system magnifications corresponding to object-to-recording system distances (o.r.d.) of 1 and 5 cm.

These investigators reported the following conclusions: At an o.r.d. of 5 cm, the Lo-Dose/long-cone (L) technique had an overall system MTF comparable to or better than the RP/M/short-cone (M) technique; at an o.r.d. of 3 cm, the two techniques have similar system MTFs; at an o.r.d. of 1

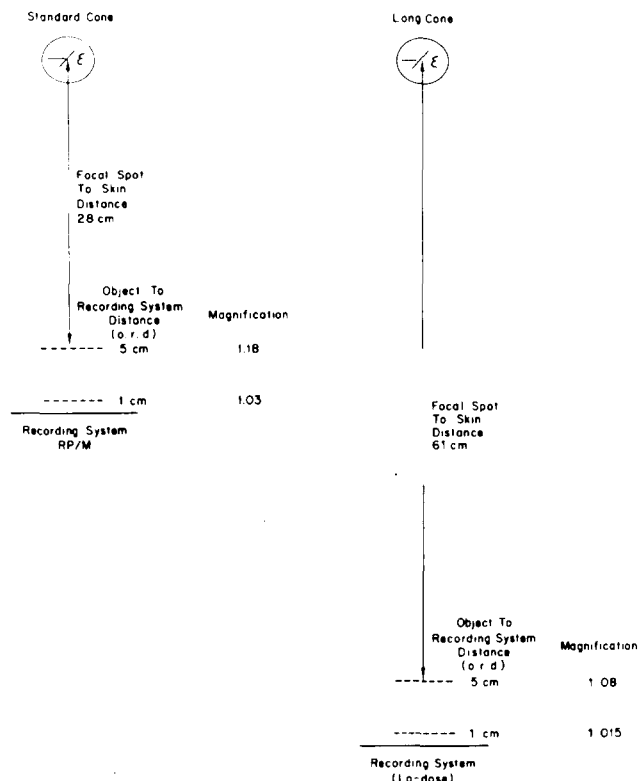


FIG. 9. Geometries and associated magnifications for standard-cone and long-cone techniques for mammography, as discussed in text and Ref. 38 (courtesy of A. Haus *et al.*).

cm, the MTF of the M system is superior to that of the L system; at all o.r.d.s, the images made with the L system appear more equal in sharpness.

A straightforward interpretation of these results is possible using the aperture theory. The aperture diameter for the x-ray-tube focus employed by the previous workers is estimated from the LSFs given by them to be about 1.1 mm. The aperture diameter for the Lo-Dose screen system is estimated from the measured MTF to be approximately 0.15 mm, using Eq. (14) in polar form. These apertures can be combined into an effective aperture in the plane of the object as a function of magnification M using the relation

$$a_{\text{object plane}} = M^{-2}[(M-1)^2 a_{\text{focal spot}} + a_{\text{screen}}], \quad (22)$$

derived in Part I by considering the scaling depicted in Fig. 10, where $(d_1 + d_2)/d_1$ is the system magnification M .

The system aperture diameter δ corresponding to the aperture (circle) calculated from Eq. (22) is given as a function of o.r.d. (using the appropriate geometry for each system) in Fig. 11. Greater values of δ correspond to greater unsharpness. The conclusions drawn from this figure are qualitatively in excellent agreement with those drawn by the previous workers; the quantitative agreement is also very good. Indeed, we used the data of these workers. (This treatment assumes that the gammas of both systems are matched.) However, if the appropriate system apertures were available from manufacturers, much insight into the possibilities of combining various system components could be obtained before the fact using simple algebra, without time-consuming computer simulation and experimentation.

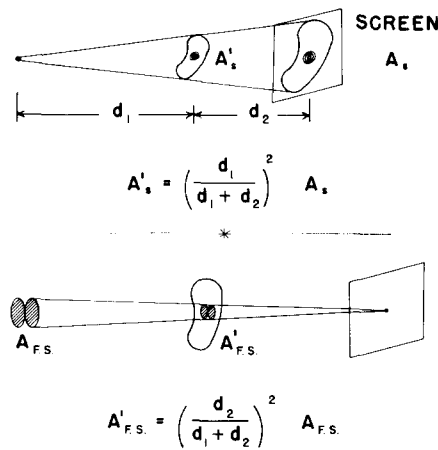


FIG. 10. Geometries for scaling focal-spot aperture and screen aperture to object plane.

VII. DETAIL SIGNAL-TO-NOISE RATIO

We are now in a position to construct the detail signal-to-noise ratio as used by Schade.⁶ This requires first the ratio of input contrast to noise contrast; this is then reduced by the detail contrast reduction factor:

$$\begin{aligned} \text{SNR}_\Delta &= [C_{\text{in}}/(Na_i)^{-1/2}](a_o/a_i) \\ &= C_{\text{in}}(Na_i)^{1/2}a_o/a_i. \end{aligned} \quad (23)$$

The film gamma does not appear since, for the low-contrast signals we will consider, it operates on both the signal contrast and the noise contrast. In taking the area of the image as the sampling area for noise, we are assuming a kind of idealized matched filtering. (This result is analogous to more rigorous expressions derived from signal detection theory, or statistical decision theory. See Ref. 3 for a summary of such results.) This is not quite realizable in practice; however, let us see how far we can go with this assumption.

If we compare Eq. (23) with Eq. (10) a modification of the Rose model is suggested. The Schade detail SNR is rewritten for the condition of threshold detection ($\text{SNR} = k$) of contrast C_T :

$$C_T = kN^{-1/2}a_i^{1/2}/a_o. \quad (24)$$

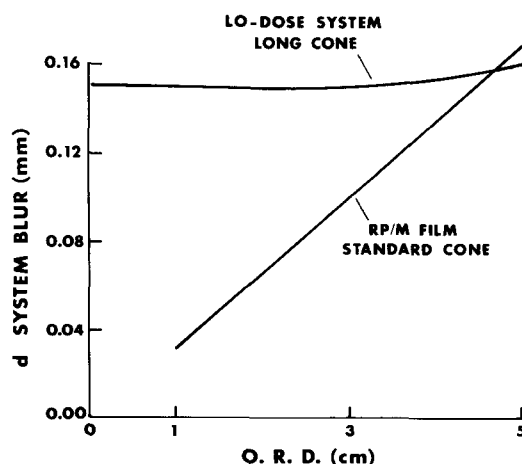


FIG. 11. System-aperture diameter as a function of object-to-recording system distance (o.r.d.) for the two techniques and geometries of Fig. 9.

TABLE IV. Sampling aperture of the eye in one dimension (mrad) as a function of background luminance (ft L) (see Refs. 6, 28, 39, 40).

| Background luminance | Schade (bars) | Schade (disks) | Schnitzler (disks) |
|----------------------|---------------|----------------|--------------------|
| 10 | 1.24 | 1.12 | 0.95 ^a |
| 1 | 1.6 | 1.44 | 1.4 |
| 0.1 | 2.42 | 2.18 | 1.95 |
| 0.01 | 3.6 | 3.24 | 2.2 |
| 0.001 | 4.65 | 4.19 | 2.55 |

^aThumb rule for radiology: Eye blur is 1 part in 1000 (of viewing distance).

For the case of the Blackwell experiment, the object area is a disk of area a_o , which subtends an angle α_o at the eye of the observer. When the disk is imaged by the eye, its effective area (aperture) is increased to a value a_i subtending an angle α_i at the eye of the observer. As above we will assume that the image area can be found by addition (areas are referenced either to object space or to the retina):

$$a_i = a_o + a_e, \quad (25)$$

where a_e is the equivalent blur area (aperture) of the eye for the given viewing conditions, corresponding to an angle α_e . From Eqs. (24) and (25) we can write

$$C_T = K' \frac{(a_o + a_e)^{1/2}}{a_o} = K \left(\frac{1}{\alpha_o^2} + \frac{\alpha_e^2}{\alpha_o^4} \right)^{1/2}. \quad (26)$$

Here we have absorbed factors of π, k , and the various luminance-level-dependent efficiencies of the eye required to find N (absorbed by the retina) into the constant K . The reason for the expansion in the second equality is to keep touch with the Rose model, Eq. (11), which does not have the second, or eye-aperture, term. Schade gives values for N_e of the eye^{6,28,39} at various levels of brightness. These are presented in Table IV in terms of their inverse, or sampling aperture in one dimension, converted to angle. These values in turn are adjusted by a factor of 0.9 for detection in the two-dimensional case (disks), based on the first entry in Table II, an *ad hoc* consideration which is not unreasonable in light of the shape of Schade's MTF curves for the eye.^{6,28}

Following Rose,²⁵ we adjust the parameter K in Eq. (26) to bring the model equation into agreement with the Blackwell data at one point (the circled data points in Fig. 12). The predictions of Eq. (26) then fall on the dashed curves of Fig. 12. As before, the Blackwell data are the points on the solid curves. We see that the agreement is excellent for small disk sizes (to the right in Fig. 12). However, for large disks, the present model equation reverts to the Rose model, and the same disagreement. The fact that the eye has a weak low-frequency response, acting essentially as an edge detector for large objects, suggests that we make the eye's sampling aperture for noise an annular ring about the object disk perimeter, for large disks. The writer has tried this using an annular ring aperture with inner and outer diameters bracketing the disk diameter, and a diameter difference equal to twice the eye's sampling aperture for the given conditions (i.e., the ring's thickness is the eye aperture). This works very well except for the largest disk diameters. Indeed, one realizes

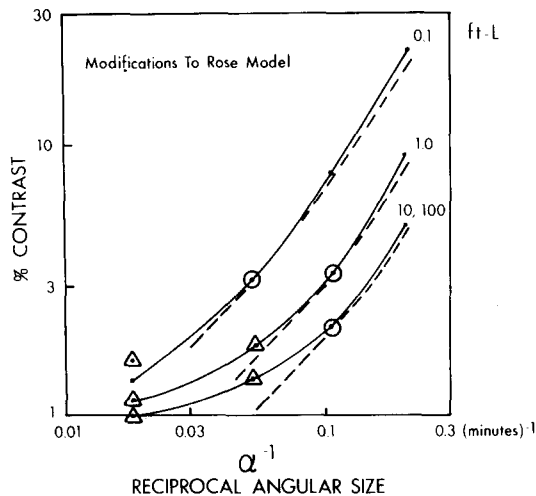


FIG. 12. Visual performance data as measured by Blackwell (Ref. 29)—points joined by solid curve. Visual performance data according to Schade's generalization of Rose model [Eq. (26)]—dashed lines. Visual performance data according to Schnitzler's generalization of Rose-Schade model [Eq. (27)]—dashed curves to right of circled point, triangles to left of it.

that such a sampling ring cannot grow indefinitely large. A more general approach is to take the lead of Schnitzler⁴⁰ and add another term—a constant—to the sum of squares of Eq. (26). This implies that there is some limiting field size over which the eye can integrate, with angular diameter α_F . The generalized sum of squares leads to the following generalized Rose model:

$$C_T = K \left(\frac{1}{\alpha_F^2} + \frac{1}{\alpha_0^2} + \frac{\alpha_e^2}{\alpha_0^4} \right)^{1/2}. \quad (27)$$

This means that for very large disks the threshold contrast takes a constant value independent of disk size. Values for α_F are taken from Schnitzler⁴⁰; they are roughly 6–8 times the value he gives for α_e (see Table IV). (In Ref. 6, Schade spoke of the same phenomenon, and estimated that this parameter was less than 14 times α_e .) This generalized model gives rise to values of C_T indicated by triangles to the left of the circled point, and dashes to its right in Fig. 12. The overall fit is seen to be excellent. Schnitzler's more complete analysis of this problem (including the temporal integration of the eye) uses more recent (unpublished) data of Blackwell. He calculates values for α_F from best fits to these data. Schade's values came from integrating the squared MTF of the eye. They are compared in Table IV and are seen to differ by only about 10% at the higher light levels, but more significantly at the lower. Typical viewboxes in radiology have brightness levels of 400–600 ft L (high-intensity light levels go to about 1500 ft L). When viewing a film with a $D_{\max} = 3$, the brightness will not be reduced to much less than 0.5 ft L. For this reason only the Blackwell data at the highest light levels are considered here; the parameters given by Schade and Schnitzler are seen to be consistent with each other and with the published data (and apparently with the unpublished data).⁴⁰

We point out here that the excellent agreement of the aperture theory with the observer data above occurs in a case where the observer knows what he is looking for and knows where to look (the Blackwell experiments).

The shape of the curve of threshold contrast versus disk diameter for the Blackwell studies and the successful application of a modified Rose theory to fit these data encourage one to attempt to apply this theory to the many examples of detail-visibility diagrams that have appeared in the literature of radiography.^{41–44} They all exhibit the bowed shape of the curves we have been studying here. However, most of the published curves leave the reader frustrated because of the lack of information concerning either the viewing conditions or the imaging systems. (Two interesting papers by Spletstosser^{45–46} on detail-visibility with industrial x-ray film may help to close this gap. The more recent reference contains some important observations concerning viewing conditions.) The most encouraging paper, in the sense of completeness of information, is that of Sturm and Morgan.⁴¹ The writer has attempted to fit their observer data in the spirit of the above model. Reasonable agreement was achieved, but deviations between the data and the model for contrast thresholds were often as great as 40%. Consolation was taken from the paper by Burger,⁴⁴ who showed considerable variation from observer to observer in the generation of a detail-visibility curve. This indicates the need to sensitize and stabilize observer response and gather a significant quantity of data if observer performance and objective measurements are intended to be rationalized. Blackwell's observers were *veterans* of from 35 000 to 75 000 observations when his reported studies were *begun*; his reported data are the results of hundreds of thousands of observations.

We next use the expression for the detail SNR given above to calculate a figure of merit for radiographic screen-film systems for the imaging of small low-contrast detail. We will need values for N to make this calculation.

VIII. THE (APPARENT) SAMPLE NUMBER

The sampling aperture of an image receptor was found from the characterization of its image spread properties, e.g., the LSF or MTF. The sample number utilized by an image receptor is found from the characterization of its noise properties, e.g., the Wiener spectrum (WS). This is a spatial frequency decomposition or spatial frequency analysis of the variance of the density fluctuations σ_D^2 or *relative* transmission fluctuations $\sigma_{\Delta T/T}^2$ in the case of a photographic or radiographic film. A complete analysis of these fluctuations involves consideration of film granularity, screen-structure granularity, the finite number of x-ray quanta utilized by the screens, and the fluctuations in the available energy per quantum absorbed. (This latter set of fluctuations is relevant since a screen-film system is not quite capable of photon counting—the light scintillations are integrated, not counted by the film. The difference in the resulting noise is small but significant, consisting of contributions from the polyenergetic spectrum, K -fluorescence escape, and fluctuations in the screen amplification gain due to geometrical path differences and mixing of phosphors with differing brightnesses with respect to film sensitivity.) A complete analysis of all these factors is yet to be carried out; when it is, it will doubtless depend heavily on the work of Doi⁴⁷ and Swank.^{48,49} (Reference 22 summarizes the state of the question.)

TABLE V. Noise-equivalent quanta NEQs in the film plane and in the object plane for a number of screen-film systems used to image a test phantom. Average sampling diameter of the focal spot was 0.35 mm. "Visibility" rating according to three observers is given in right-hand columns. Schade detail signal-to-noise ratio SNR_{Δ} calculated according to Eq. (23) is given in fourth column from right. (Plus signs in NEQ columns are suggested by Weiner spectra that cross in the low spatial frequencies (see Ref. 50). SNR_{Δ} and "visibility" for 1 mm seeds ($C = 2.5\%$).

| Screen-film | M | NEQs (film plane) | NEQs (object plane) | SNR_{Δ} | RFW | EWD "visibility" | RES |
|---------------|-----|-------------------------------|--------------------------------|----------------|-----|---------------------|-----|
| Lanex/Ortho G | 2X | $3.6 \times 10^4/\text{mm}^2$ | $14.4 \times 10^4/\text{mm}^2$ | 7.4 | 5 | 5 | 5+ |
| Alpha 4/XM | 2X | 0.9+ | 3.6+ | 3.8+ | 4 | 3.6 | 5- |
| Alpha 8/XM | 2X | 0.9 | 3.6 | 3.7 | 3+ | 3 | 3+ |
| Par/RP | 1X | 4.5 | 4.5 | 4.1 | 3+ | 3 | 3 |
| Lanex/Ortho G | 1X | 3.6 | 3.6 | 3.2 | 3 | 2.5 | 2 |
| Alpha 4/XM | 1X | 0.9+ | 0.9+ | 1.8+ | 1+ | 1.3 | 1+ |
| Alpha 8/XM | 1X | 0.9 | 0.9 | 1.6 | 1 | 1 | 1- |

The complete analysis is not required for image evaluation, however, since what is seen is the synthesis of the individual effects. One can attribute the measured fluctuations to the fluctuations that would have resulted from the counting of a smaller number of equivalent quanta, the so-called noise-equivalent quanta (NEQ). (A broad treatment of the subject together with an extensive bibliography is contained in the recent book by Shaw and Dainty.⁵⁰) This is obtained by referring the density or relative transmission fluctuations to the exposure axis using the relations

$$\sigma_D^2 = (0.43)^2 \gamma^2 \sigma_{\Delta E/E}^2, \quad (28)$$

$$\sigma_{\Delta T/T}^2 = \gamma^2 \sigma_{\Delta E/E}^2,$$

which hold for small fluctuations [scale factors are from Eqs. (4) and (5)]. Since the WS Φ_D , $\Phi_{\Delta T/T}$ are decompositions of the respective σ^2 , the same scale factors relate them to $\Phi_{\Delta E/E}$. Finally, the WS of the relative exposure fluctuations (quanta or roentgens) is equal to $1/N$, the inverse of the equivalent quantum flux. We then obtain

$$N = (0.43)^2 \gamma^2 / \Phi_D, \quad (29)$$

for constant Φ_D , or at $\Phi_D(0)$, and a similar relation involving $\Phi_{\Delta T/T}$ with the numerical constant divided out. This would hold for a wide band of frequencies up to some limit determined by the aperture of the instrument used to measure the WS, if the image receptor had no aperture effect. Since the typical screen-film system has an aperture effect detectable down to the lowest measurable spatial frequencies (a fraction of a cycle per millimeter), this relation is very difficult to use in practice. The author has taken data published by Doi,⁵¹ and data obtained in our own laboratories,^{52,53} and extrapolated the WS back to zero spatial frequency in order to apply Eq. (29). (We measure Φ_D ; Doi measures $\Phi_{\Delta T/T}$. Absolute noise levels and errors are determined as described in Ref. 22.) This is subject to large errors (of order 20%–10% effect on SNR in the case of our own data where the bandwidth, dictated by time and optical considerations, has a value 0.45 cycles/mm: This is relatively large for the calculation described here.) The resulting estimates of N or NEQ, the noise-equivalent quanta, for a number of screen-film systems exposed to a film density of 1.0 with an 80-kVp, 7.0-mm-Al HVL beam (19-mm-Al absorber added at tube), are given in Table V.

A partial explanation of these numbers can be attempted.

If the only source of noise in radiography were x-ray quantum noise, the ratio of NEQs for various systems would be determined by their relative absorption/speed ratios. For example, within the calcium tungstate technology a speed gain of a factor of 2 is often achieved by an absorption gain of about the same amount (say, DuPont Par, 21%, versus DuPont Hi-Plus, 39%—see Refs. 52 and 53). When this is the case, the low-frequency noise and the NEQs are about the same—doubling the absorption, halving the flux leads to the same number of utilized quanta. The ratio of 3.6/4.5 for the Lanex versus the Par system is then explained mostly by their relative absorption/speed ratio 3.5/5.0: Lanex absorbs about 3.5 times more photons for this beam quality than Par; the Lanex system has about 5 times the speed of the Par/RP system.⁵³ The ratio of 0.9/4.5 for the Alpha 8 versus the Par system is explained mostly by their relative absorption/speed ratio 2.5/10: The 50% absorption by Alpha 8 is 2.5 times that of Par; Alpha 8/XM is about 10 times as fast as Par/RP. The ratio of almost unity for the Alpha 4 versus Alpha 8 system is puzzling. They have almost the same absorption; Alpha 8/XM has 1.6 the speed of Alpha 4/XM (Alpha 4 contains an acutance dye). One would expect the Alpha 4 NEQ value to exceed 1.4. The measurements indicate that it is no greater than 1.2. The discrepancy is currently ascribed to experimental error and the difference in K -fluorescence escape between the two. K -fluorescence escape is another source of fluctuation or noise (our early Alpha 4 contained only Gd; Alpha 8 contained Gd and La; some Alpha 4s now contain Gd and La).

We now have all the information required for the analysis of an interesting radiographic experiment.

IX. A SYSTEMS ANALYSIS

In our laboratories we use a phantom comprised of a variety of high- and low-contrast, one- and two-dimensional structure for the subjective evaluation of radiographs. One section of the phantom contains over 20 spherically shaped birdseeds ranging from 0.5 to about 1.8 mm in diameter, glued to a thin plastic support. This phantom was radiographed with a number of screen-film systems using a Machlett Dynamax 66 biased 0.3-mm nominal focus and geometry of 1X (contact) and 2X magnification. The radiographs were taken at 80 kVp, with 19-mm-Al absorber added at the tube to simulate an average diagnostic beam.⁵⁴

The magnification radiographs were photographically reduced to a 1 \times presentation; the 1 \times radiographs were reproduced one to one with the same optics. The writer and two colleagues then independently ranked the final images in order of visibility of small birdseed and scored them on a scale of 5 (highest) to 1. The ranking and scores are given in Table V (we found it necessary to add partial steps in scoring the images). There was undoubtedly some prejudice in the minds of the observers and a certain lack of detachedness due to an accumulation of experience with these systems. However, we attempted to give fair ratings based on careful comparisons of the images. This is clearly not the best psychophysical experiment that can be designed, yet it is the *kind of comparison most frequently used* by those doing subjective image-quality evaluation.

After the scoring was completed, the writer calculated the detail SNR for the systems using Eq. (23). The exposure contrast was estimated as 0.025 using a film exposed with detail screens. The number of NEQs is the number in Table V (given in the film plane) times the magnification squared M^2 , giving the density of NEQs in the object plane. (Implicit in this analysis is the assumption that the statistics in the image are efficiently coupled into the eye. This is a reasonable assumption whenever the image noise is easily perceived.) The object aperture was taken to be that of a 1-mm-diameter sphere (equivalent aperture diameter = 0.94); this was cascaded with the system blur diameter calculated according to Eq. (22). The aperture diameter of the focal spot (in its plane) was estimated to be 0.35 mm, based on pin-hole images and the star-phantom image. The equivalent diameters of the aperture functions of the screens were estimated from values of N_e calculated from the WS measurements referenced above. Since these estimates are quite rough (error may be of order 25%) they will not be published here until better estimates are made from MTF measurements. (A similar reservation was not made in the case of the NEQ; the estimates given for this quantity may be the best available for some time. The reader may deduce the N_e 's used here by checking the calculation of SNR.) We merely state that the value of the parameter d used for (3M) Alpha 4 screens is in the neighborhood of the value given in Sec. VI for Par screens; for (Kodak) Lanex Regular and (3M) Alpha 8 screens the value used is in the neighborhood of that given in Sec. VI for TF-2 screens. The effect of the rough estimates is to introduce errors in the calculated SNR that are less than 8%. The aperture diameter of the eye was not cascaded into the calculation of a_i since we allowed ourselves to view the images carefully at any distance; the aperture diameter of the eye became as low as 0.20 mm and would therefore have a negligible effect on the resulting SNR. Finally, a more exact treatment would involve separating the NEQs into two components—quantum mottle and film granularity. Only the first component is sampled by the total-system aperture (see Ref. 28 for more complicated examples). Here we make a small error by neglecting this distinction—the error is negligible in the context just described.

The detail SNRs calculated for the various systems are given in Table V. Although the parallel with the ratings given by the observers is remarkable, we must point out that the

considerations of the last paragraph require a SNR difference of about 10%–15% in order to be considered significant. However, we conclude that up to this point there is nothing inconsistent in this simplified approach and the promise offered by it is worthy of serious consideration. Moreover, the test conditions and test phantom seem quite suited to signal *detection* experiments since the resulting SNRs (1–7) include the range generally considered necessary for threshold detection (2–5). (The above experiment was concerned strictly with *visibility*, since quite a bit of *a priori* knowledge was available to the observers.) Finally, we point out the inadequacy of the test phantom for rating higher-quality images. The doubling of the detail SNR between the next highest and highest case was not reflected in the rating value given by an observer. (Afterwards, we all agreed that the system with the highest detail SNR had greatly reduced noise content.) It appears that, once the SNR is above some value in the neighborhood of 4, the “visibility” is not enhanced proportionately by further increases in SNR (when you know where to look).

In the above study the SNR was dominated by $(\text{NEQ})^{1/2}$. The variation of the value of NEQ over a range of 16–1 overshadowed differences in the overall system passband—the latter were first-order corrections. We shall now see that, when the major difference in systems is their passband, it is more difficult to rate them under noise-limited conditions.

X. THE PROBLEM OF THE SEARCH

In the SNR of Eq. (23) the image area a_i is calculated as $a_o + a_s$, the sum of the object aperture plus the aperture of the system that produces the blurring. It is clear from Eq. (23) that, for a given contrast, object area, and NEQ per unit area, the best imaging system is the system with the *smallest blur aperture*, i.e., the sharpest system. Immediately after this expression was given, we pointed out that we were assuming the viewer of the image could integrate the signal flux (i.e., apparent signal flux) over an area the size of the actual image. From this assumption we were able to explain the Blackwell contrast thresholds for gray disks and could calculate useful SNRs for detail visibility in radiographs. In these examples and in the examples of the references of Sec. VII dealing with detail-visibility diagrams, generally the viewers knew the pattern of the target disks—i.e., where to look and what to look for. There is one outstanding piece of data for an experiment in which the viewer knew what he was looking for, but didn't know where to look. Let us see how it follows our model.

Goodenough^{55,56} conducted an experiment on the detectability of a low-contrast, 2-mm-diameter plastic bead as imaged with four radiographic screen–film systems: a medium-speed film (Kodak RP) with medium-resolution screens (DuPont Par) and “fast-” resolution screens (Radelin TF-2); and a fast film (Kodak RPR) with the same sets of screens. For each film–screen combination listed, 100 radiographs were made: 50 of these were just “uniform” exposures with no bead present; 50 of them had one bead placed at random in the field. From the observer's performance and rating of his degree of certainty about the presence or absence of the

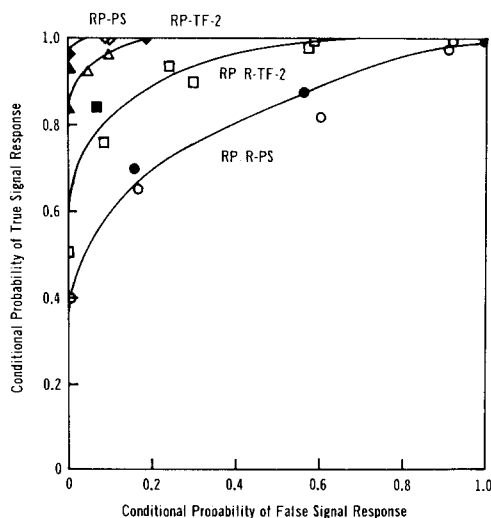


FIG. 13. Family of receiver operating characteristic (ROC) curves for the detection of a low-contrast 2-mm-diameter plastic bead as imaged with four radiographic screen-film systems (courtesy of D. J. Goodenough; see Refs. 55, 56).

bead, Goodenough developed the so-called receiver operating characteristic (ROC) curve—this is a graph of true positive (TP) responses versus false positive (FP) or false-alarm responses. A typical example from this work is given in Fig. 13. Better performance is characterized by a curve close to the upper-left-hand corner of the graph; guessing is characterized by the positive diagonal. We see that with the medium-speed film (RP) better performance was obtained when the *sharper* screens were used (Par); with the fast film (RPR) better performance was obtained when the *less sharp* screens were used (TF-2). Now, all of the author's noise measurements indicate that, for a given film, these two screen systems utilize about the same number of NEQs (to within 20%). If this is so, then the above analysis would predict better performance using the sharper screens. Whatever the physics of the situation, a reversal of performance such as we have here is difficult to explain without looking into the eye (brain) of the beholder.

For the moment let us ignore the amazing ability of the eye-brain to integrate counts over an area the size of the object or its image. Let us assume that the eye has the aperture properties of a simple scanner with the same blur diameter as the eye. For the ROC experiment above, the viewing distance was fixed at 20 in.; the illumination, between 125 and 200 ft L; film density about 0.7. From Table IV we see that the aperture diameter of the eye for two-dimensional sampling under these conditions is approximately 0.50 mm. From Sec. VI, the aperture diameters of Par and TF-2 screens are 0.38 mm and 0.65 mm, respectively (incorporating the 0.9 factor of Table II). This gives a system aperture (eye plus screen) of 0.63 mm for Par and 0.82 mm for TF-2 screens. Now, for a simple scanner, the detail SNR becomes

$$\text{SNR}_{\text{scan}} = C_{\text{in}}(Na_{\text{sc}})^{1/2} \frac{a_o}{a_o + a_{\text{sc}}}, \quad (30)$$

where a_{sc} is the sampling aperture of the scanner. If we treat the system of eye plus screen as the scanner, then in this

model (for the case of 2-mm bead) the system of eye plus TF-2 screens has a SNR 22% higher than the system of eye plus Par screens. (The statistical factor favors TF-2 by 30%; the contrast reduction factor favors Par by only 7%.)

Now we have two models that give two different answers: If the eye can integrate over the image area, the *sharpest* system will lead to superior performance; if the eye is forced to operate in a scanning mode and can only integrate over the blur aperture (eye plus display), the *unsharp* system leads to superior performance. In the light of the two models, and the observed reversal in performance, the author suggests the following holding pattern. When the observer knows just what to look for and where to look he appears to be able to integrate over the entire object or image area and get the full benefit of the available statistics—this is borne out by the Blackwell data and the applicability of the Rose model (with modifications) to this data. However, an additional feature of the Blackwell experiment is the fact that the automatic gain control mechanism of the eye appeared to be set at a level that limited the perception of the statistical fluctuations that set the fundamental limits to perception—the noise is not perceived except at the lowest lights.⁷ In the bead detection experiment of Goodenough, the observer has to *scan* a field that is very noisy, and to *search* for a hint of the presence of a bead and to compare this to the rest of the field. It may be difficult to tune to object-sized areas for statistical sampling in such a case. In fact, sometimes the bead signal is manifested as a “blip” much smaller than the bead area (more below). In this complicated search or scanning task, the eye-brain may only be capable of achieving the SNR of a scanner with an aperture equal to the blur aperture (eye plus display). For lower conditions of noise and therefore less complicated search, or where the search is trivialized since the position of the signal is indicated, the eye is able to integrate over the object area and get the full benefit of the statistical information presented—*without paying the price of a scanner with the same integrating properties, which would blur the signal with the same aperture, thus degrading the SNR*. The implications of this tuning and associated difficulties are important for estimates of exposure requirements: For the case of the 2-mm bead above, the SNRs calculated with Eq. (23) are about 3 times as great as those calculated with Eq. (30) for the scanner; this can lead to an estimate of required exposure that is too low by almost an order of magnitude if Eq. (23) is used but the viewing is complicated by a search. Moreover, the larger the field, the more complicated the search for a given object—and there are more opportunities for false positives. Goodenough and Metz⁵⁷ have worked out the probabilities of detection (defined as 50% TP rate, and 10% or 20% FP rate) of a signal in noise as a function of a simplified SNR and the number of independent object-sized areas that must be scanned in a simplified search strategy. These probabilities are given in Fig. 14 as a function of the number of independent areas, M . Almost a fourfold increase in the SNR (16-fold increase in exposure) is required as the number of areas increases from 1 to 1000. Again, a *caveat* on the ease of underestimating required exposure for even a simple task.

The implications for image display are also obvious, but

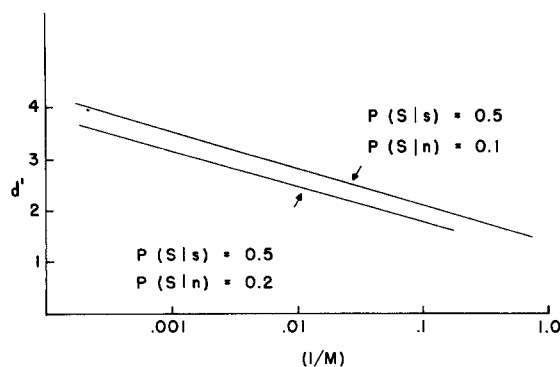


FIG. 14. Simplified SNR d' required for detection (defined as 50% TP rate, and 10% or 20% FP rate) of a signal in noise as a function of the number of independent object-sized areas, M , that must be scanned in a simplified search strategy in the model of Goodenough and Metz (Ref. 57) (courtesy of D. J. Goodenough).

difficult to quantify: If the amount of image blurring is adjustable the detection rate may improve, as in the above case of unsharp screens (see, e.g., Ref. 58). A simple way to vary such tuning is to adjust one's viewing distance. This has been pointed out several times in the literature for radiologists.^{59,60} However, the emphasis has been placed on eye MTF, not noise integration.

The SNR of Eq. (30) for a scanner has a maximum when the sampling area of the scanner is equal to the object area (this is a simple way to derive the matched-filter result). This condition holds for the 2-mm-bead experiment when the viewer maintains a distance of about 2 m for films made with Par screens and 1.9 m for films made with TF-2 screens. We are using here the result in Table IV that for normal viewing the eye's aperture is approximately 0.001 rad. Russell Morgan,⁵⁹ using data for the MTF of the eye and a different criterion, concluded the optimal viewing distance was about 300 times the object size. (Our rule here—1000 times—is approximately the same as the conclusion of Schade.²⁸) However, again we must take great care in using any such result. If the eye is able to integrate the noise in an object-sized area without additional blurring, as in the experiments where the noise is unobtrusive, any additional blurring from distant viewing would be detrimental. The SNR calculated from Eq. (23) (modified Rose model) for the case of the 2-mm-bead experiments is almost twice the value calculated from Eq. (30) (scanner) for the conditions of *matched viewing*! The eye can beat the *matched* filter because it can integrate (associate areas on the retina) without blurring. The *optimal* filter can beat the eye because it can associate or integrate counts, without blurring, and without running out of area in which to integrate. At present, however, there is little threat to the eye from any extant beast (e.g., computerized scanner).

The above range of performance will be extremely difficult to quantify in any single expression. The author believes the whole business is extremely dependent on the noise context. More generally the noise is not just quantum fluctuations but also unwanted signal or clutter. The Temple University group refers to this as structured noise.⁶¹ In a particular experiment of theirs using a simulated 8-mm chest lesion, the optimal

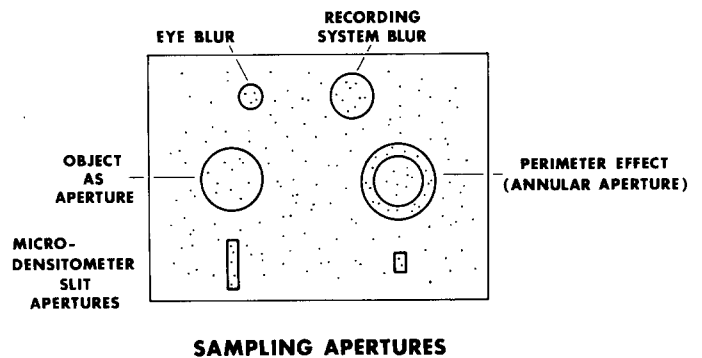


FIG. 15. For an instrument such as a microdensitometer, the sampling aperture for noise is straightforward to deduce. For the human eye involved in a search task, the aperture can range from the eye blur (Morgan model) to the object aperture (Rose model).

viewing distance was found to be around 2 ft,⁶⁰ less than the above rules of thumb would suggest.

An intuitively appealing approach to a unified view of this complicated subject has been suggested to the writer by Dr. Gertrude Kornfeld of the Night Vision Laboratory at Fort Belvoir, Virginia. Dr. Kornfeld believes that in a noisy display the eye builds up signal during a search according to the Morgan model. [The aperture for noise is the eye aperture—as with the scanner of Eq. (30).] Only after the stimulus has been built up can the eye approach the optimal operation of associating counts within the object area and follow the Rose model (see also Ref. 62). Quantification of this will have to include the fact that the contrast threshold for noise visibility is *lower* than that for signal visibility (by at least a factor of 26.²⁸). (The author has noticed that small beads, just barely visible at close viewing, appear larger at increased viewing distances. Apparently, at the larger distances the noise contrast is below threshold and therefore no longer competes with portions of the object signal. This emphasizes the need to incorporate noise levels into any consideration of optimal viewing distances.) The range of possibilities is suggested schematically in Fig. 15. To the writer, the central question in the analysis of observer performance studies concerns this range of possibilities and its relation to noise level and complexity of search.

XI. THE NOISE-FREE LIMIT

There are a number of cases in radiology that can be considered to be not limited by noise:

(a) The noise is not easily seen, as in the case of direct-exposure x-ray film exposed to normal densities and viewed under normal conditions. (This suggests that the internal noise of the eye is somewhat above this level.) The density of NEQs is on the order of $100 \times 10^4/\text{mm}^2$, compared to the values of $(1-5) \times 10^4/\text{mm}^2$ for ordinary radiography. The former high values are comparable to those encountered in aerial reconnaissance photography. (A review of photographic parameters for various applications is given in Ref. 22.)

(b) The object area is sufficiently large so that, even though the noise is plainly visible, the noise contrast calculated over the object area is small compared to the object

contrast. This may be seen when objects on the order of 1 cm in diameter are radiographed with direct-exposure film, and also with screen-film systems. Even though the latter give noisier radiographs, they have no difficulty imaging large objects with exposure contrasts on the order of 1% in the absence of scatter.

(c) The object contrast is about an order of magnitude greater than the noise contrast (again, integrated over the object area), so that we *no longer have a case of signal detection*. This may be the case with the blood-vessel images considered by Rossmann,^{35,36,63} where, for matched system speeds, the sharp noisy images (Par/RPR) were preferred to the unsharp lower-noise images (TF-2/RP).⁶⁴ The writer believes that this is an area for further investigation. If one calculates the SNR using Eq. (23) for images of a long, fine blood vessel made with the two systems just listed, one finds that the lower-noise image should have a slight edge. (The reader can check this easily using the blur sizes given earlier and the fact that the NEQ for the RPR system is about half that for the RP system.⁵³) There are two ways out of this apparent difficulty: The blood vessels that are imaged may have a SNR in excess of the detection threshold, yet may have contrast levels that are close to the visual threshold of contrast detection (Sec. V). What is required is contrast, not SNR, and this is provided by the sharper system; also, the detection of a blood vessel in a noisy background is not a trivial signal-detection task—recognition is also involved, and a higher-contrast, piecewise noisy image may be easier for the eye-brain to recognize than a lower-contrast less noisy image. Finally, the likelihood of noise mimicking or masking a long vessel can become vanishingly small in the above example.

An evaluation of such contrast-limited images is generally made on the resultant overall contrast. This can be expressed in terms of the point gamma of the image receptor and its MTF. Before we consider this, we mention that many photographic investigators calculate a quantity called *acutance* as a figure of merit; acutance has been found to correlate well with the subjective impression of photographic sharpness. It is defined as the mean square value of the gradient $Q'(x)$ of the density distribution across an edge trace, within certain limits, normalized to unit density difference.⁶⁵ Schade⁶⁶ has indicated the relation between N_e and such averages; in particular,

$$N_e = \frac{\int [Q'(x)]^2 dx}{[\int \text{LSF}(x) dx]^2},$$

for a gamma of unity (this is a straightforward consequence of Parseval's theorem). A more general treatment⁶⁷ indicates that acutance is proportional to the product of gamma and N_e . (One might guess that it would involve gamma squared—this psychophysical quirk is another hint of nonlinearity in the visual system.)

The product of gamma and the MTF has been used in radiology as a generalization of the MTF.⁶⁸ It may just as well be considered as a generalization of gamma to include higher frequencies. Shaw⁶⁹ takes the latter point of view in his use of this product [the so-called contrast transfer function (CTF)] for an evaluation of the xeroradiographic image, with its characteristic low value of large-area contrast transfer (γ

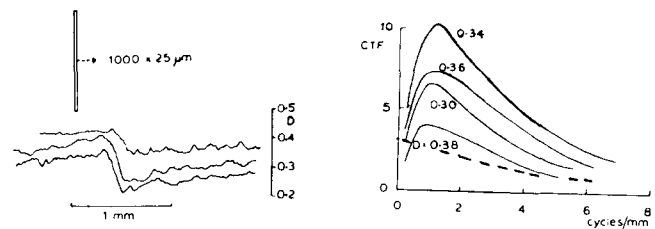


FIG. 16. Contrast transfer function (CTF) for the xeroradiographic image (solid lines) and for a high-resolution screen-film system such as the type used in mammography (dashed line) (courtesy of R. Shaw; see Ref. 69 for details).

≈ 0.2) and very high gain in the midfrequency region (see Fig. 16). At this point it would appear reckless to apply the aperture theory to such a complex imaging characteristic. However, it is not out of the question. N_e is a one-parameter measure of the transfer characteristics of a low-pass filter. The xeroradiographic process is a combination of a low-pass filter and a high-pass filter with high midfrequency gain. An N_e approach might be useful to characterize the low-pass filter. The high-pass filter might be a characterization analogous to the Schnitzler treatment of vision of large disks considered above, or Schade's treatment of a high-pass filter as the combination of a constant and a negative low-pass filter. These questions invite further investigation.

XII. NONLINEARITY ALONG THE FREQUENCY AXIS

Nonlinearity of transfer characteristics was treated by an approximate method in Sec. II. There is another nonlinearity that must be considered and which is suggested by the following observations.

(a) With many of the senses the just noticeable difference (jnd) is roughly a constant fraction of the background, leading to descriptions of the senses in logarithmic terms. This may be the case with spatial frequency; it has led certain authors to specify an image-quality index in terms of an integral along the log frequency axis.^{70,71}

(b) The critical band within which noise is effective in masking spatial frequency information is specified in terms of octaves, a log frequency concept.^{72,73}

(c) The edge enhancement capability of the eye cannot readily be appreciated from MTF-type descriptors of the eye unless they are presented on a log spatial frequency axis.^{6,74-76}

These points (as well as the fact that the electrostatic imaging systems used in radiography⁷⁷⁻⁸¹ are capable of giving MTF-type descriptors resembling that of the eye) call for extreme care in applying Fourier techniques to any general analysis of image quality for systems involving a human observer. It is the opinion of the writer that the aperture theory of Schade works as well as it does because integrals of the squared MTF of such devices tend to weight the low-frequency response heavily, as would happen if one were to use a summary measure involving an integral along the log spatial frequency axis.⁷⁰

(As of this writing, several new studies by Schnitzler have appeared which may have an impact on how the next gen-

eration of techniques for evaluating imaging systems involving human observers may proceed.^{81,82}

XII. CONCLUSION

The aperture theory of Otto Schade provides a unified context for an approximate treatment of noise-limited images in radiography. Its power resides in the broad utility of a single quantity derived from the MTF—the sampling aperture—to describe unsharpness, and noise sampling. A quantity derived from noise measurements, the noise-equivalent number of quanta (NEQ), is used together with the sampling aperture to determine noise contrast or the signal-to-noise ratio. Results were obtained which are consistent with more elaborate analysis and with the fundamentals of statistical decision theory. There are many unsolved problems, however, involving the human observer. The writer agrees with the assessment of the current status given by Kurt Rossmann: "In the last ten years, our basic knowledge of the physics of radiologic imaging has increased to such an extent that it cries out to be linked with observer performance studies.⁸³" This link will be very difficult to make through elaborate signal-detection theoretic integrals unless a first-order set of approximations can be made to indicate what the integrands might be. This paper indicates that a set of approximations exists in the nonmedical literature which provides both a context for unifying what we already understand and a vocabulary for asking questions about matters which we don't. Our hope is that a further synthesis of investigations in radiology with those in non-medical imaging areas may bring us closer to the goals which we hold in common.⁸⁴⁻⁸⁸

ACKNOWLEDGMENTS

Any attempt to list the many investigators with whom I have had helpful discussions during the course of the work reported here would read like the list of references and would risk serious omissions. I am deeply grateful to you all for some excellent exchange. Since charity begins at home I must express my sincere appreciation to the Director and staff of the Division of Electronic Products (DEP) (essentially the engineering and physics laboratories of the BRH) for your constant support during this work. Finally, I think it is obvious that my greatest source of inspiration has been the work of Otto H. Schade, Sr., and some very stimulating discussions with this unique gentleman, master of theory and experiment. Paraphrasing Chesterton, one can truly state that it is not a question of Schade's ideas having been tried and found wanting in radiology, they have never really been tried. I hope we can remedy this.

[Notes added in proof: (1) Calculations by A. E. Burgess, based on more accurate MTF data than that available to the author, result in values of sampling apertures for screens in very good agreement with those given here, with the exception of the value given here for TF-2 screens, which represents a significant overestimate as suggested in Sec. VI. Burgess' work has been submitted for publication. (2) The x-ray-tube focal spot does not color x-ray quantum noise; therefore one

might question the inclusion of its blur effect in the numerator of Eq. (23) (i.e., quantum noise is inserted *after* focal spot blurring, but *before* screen blurring). Nevertheless, the literal application of Eq. (23) is not arbitrary. The Schade SNR has been derived from statistical decision theory in a manuscript just completed by the author, and is shown to correspond to optimum performance by the decision maker.]

^{a)}Presented at the Fourth International Conference on Medical Physics, Ottawa, Ontario, Canada, July 1976.

^{b)}Most expressions in this work are zero- or first-order approximations. Any next-order operations (such as differentiation to obtain optima) will be meaningless or, at best, zero-order approximations.

¹C. A. Mistretta, *Opt. Eng.* **13**, 134 (1974).

²K. E. Weaver, R. F. Wagner, and D. J. Goodenough, Eds., *Medical X-Ray Photo-Optical Systems Evaluation*, Proc. SPIE (SPIE, Palo Verdes Estates, CA, 1975), Vol. 56; HEW Publ. (FDA) 76-8020 (U.S. GPO, Washington, DC, 1975).

³R. F. Wagner and K. E. Weaver, *Proc. SPIE* **35**, 83 (1973).

⁴O. H. Schade, *J. Soc. Motion Pict. Telev. Eng.* **56**, 137 (1951).

⁵K. Doi, H. K. Genant, and K. Rossmann, *Radiology* **118**, 189 (1976).

⁶O. H. Schade, *J. Opt. Soc. Am.* **46**, 721 (1956).

⁷A. Rose, *Vision: Human and Electronic* (Plenum, New York, 1973).

⁸R. F. Wagner and K. E. Weaver, *Radiology* **118**, 183 (1976).

⁹A. L. Luiten, "Activities and Trends in the Development of X-Ray Image Detection and Handling Systems," *Future of Medical Imaging*, Inst. Graphic Commun. Conf., November 1974. Private communication from Philips Medical Systems, Inc., Shelton, CT.

¹⁰A. L. N. Stevels, *Medicamundi* **20**, 1222 (1975).

¹¹J. W. Castle, *Proc. SPIE* **70**, 212 (1975).

¹²H. M. Cleare, "General Physics of X-Ray Film-Screen-Process Speed and Contrast Characteristics," in *Medical X-Ray Photo-Optical Systems Evaluation*, Proc. SPIE, edited by K. E. Weaver, R. F. Wagner, and D. J. Goodenough (SPIE, Palo Verdes Estates, CA, 1975), Vol. 56, pp. 4-7.

¹³K. E. Huff and E. C. Shaffer, "Status Report of ANSI PH2.31 Task Force on Sensitometry of Screen-Film-Processing Combinations," in *Medical X-Ray Photo-Optical Systems Evaluation*, Proc. SPIE, edited by K. E. Weaver, R. F. Wagner, and D. J. Goodenough (SPIE, Palo Verdes Estates, CA, 1975), Vol. 56, pp. 19-25.

¹⁴T. R. Fewell, private communication.

¹⁵C. Jaffe and E. W. Webster, *Radiology* **116**, 631 (1975).

¹⁶G. T. Barnes, H. M. Cleare, and I. A. Brezovich, *Radiology* (Sept. 1976).

¹⁷R. G. Gould, thesis, Univ. Pennsylvania (1971).

¹⁸R. E. Shuping, private communication based on use of Br. J. Radiol. Suppl. No. 10 (1961).

¹⁹J. G. Bonenkamp and W. H. Boldingh, *Acta Radiol. Diagn.* **51**, 479 (1959); **52**, 149 (1959); **52**, 241 (1959); **55**, 225 (1961).

²⁰K. Reiss and B. Steinle, *Phys. Med. Biol.* **18**, 746 (1973).

²¹J. W. Motz and C. E. Dick, *Med. Phys.* **2**, 259 (1975).

²²R. F. Wagner, "Noise Equivalent Parameters for Screen-Film Systems in Medical Radiology: The Present Picture and Future Pictures," in *Image Analysis and Evaluation*, Proc. SPSE Int. Conf., Toronto, Canada, 19-23 July 1976, to be published.

²³G. U. V. Rao, *Influence of focus and off-focus radiation on radiographic detail (modulation transfer function) and patient exposure in diagnostic radiology*, report on work carried out under contract No. SAPH76496 between Johns Hopkins University and the Division of Radiological Health, U.S. Public Health Service.

²⁴K. E. Weaver, R. F. Wagner, and D. J. Goodenough, "Performance Considerations of X-Ray Tube Focal Spots," in *Medical X-Ray Photo-Optical Systems Evaluation*, Proc. SPIE, edited by K. E. Weaver, R. F. Wagner, and D. J. Goodenough (SPIE, Palo Verdes Estates, CA, 1975), Vol. 56, pp. 150-158.

²⁵A. Rose, *J. Opt. Soc. Am.* **38**, 196 (1948).

²⁶R. C. Jones, "Quantum Efficiency of Detectors for Visible and Infrared Radiation," in *Advances in Electronics and Electron Physics*, edited by L. Marton (Academic, New York, 1959), Vol. XI, pp. 87-183.

- ²⁷O. H. Schade, J. Soc. Motion Pict. Telev. Eng. **73**, 81 (1964).
- ²⁸O. H. Schade, *Image Quality: A Comparison of Photographic and Television Systems* (RCA Labs., Princeton, 1975).
- ²⁹H. R. Blackwell, J. Opt. Soc. Am. **36**, 624 (1946).
- ³⁰E. C. McCullough, Med. Phys. **2**, 307 (1975).
- ³¹O. H. Schade, J. Soc. Motion Pict. Telev. Eng. **58**, 181 (1952).
- ³²R. F. Wagner, K. E. Weaver, E. W. Denny, and R. G. Bostrom, Med. Phys. **1**, 11 (1974) (Part I). In Part I it was stated that for a square aperture the volume of the squared MTF in the central lobe is about 95% of the total. This numerical value was in error due to a mistake in a numerical calculation performed longhand; the mistake was repeated upon checking the suspiciously high value. In fact, the value is about 81%. For a round aperture the value is approximately 84%. For the realistic apertures (focal spots) considered, the value was always greater than 90%, as stated. This is due to their softer edges, compared with the binary (black/white or closed/open) apertures.
- ³³No new notation was introduced in Part I. Throughout Part I the quantity referred to as the two-dimensional N_e is equal to $N_e^{(2)}$ as used here. At this point this seems to be the simplest proliferation of notation. See Ref. 31 for the original notations.
- ³⁴O. H. Schade, Natl. Bur. Stand. Circ. 526 (1954).
- ³⁵K. Rossmann, A. G. Haus, and G. D. Dobben, Radiology **96**, 361 (1970).
- ³⁶A. G. Haus and K. Rossmann, "Effect of the X-Ray Spectrum and Screen-Film Unsharpness on the Imaging of Blood Vessels," in *Small Vessel Angiography*, edited by S. K. Hilal (Mosby, St. Louis, 1973), pp. 13-21.
- ³⁷In Part I the emphasis was on sampling areas and the two-dimensional result was used; $\delta = 0.9d$.
- ³⁸A. G. Haus, K. Doi, J. T. Chiles, K. Rossmann, and R. A. Mintzer, Invest. Radiol. **10**, 43 (1975).
- ³⁹O. H. Schade, "Evaluation of Noisy Images," in *Medical X-Ray Photo-Optical Systems Evaluation*, Proc. SPIE, edited by K. E. Weaver, R. F. Wagner, and D. J. Goodenough (SPIE, Palo Verdes Estates, CA, 1975), Vol. 56, pp. 107-114.
- ⁴⁰A. D. Schnitzler, J. Opt. Soc. Am. **63**, 1357 (1973).
- ⁴¹R. E. Sturm and R. H. Morgan, Am. J. Roentgenol. Radium Ther. **62**, 617 (1949).
- ⁴²E. W. Webster and R. Wipfelder, IRE Trans. Bio-Med. Electron. **9**, 150 (1962).
- ⁴³K. Rossmann, "Effect of Quantum Mottle and Modulation Transfer on the Measurement of Radiographic Image Quality," in *Diagnostic Radiologic Instrumentation*, edited by R. D. Moseley and J. H. Rust (Thomas, Springfield, IL, 1965), pp. 350-369.
- ⁴⁴G. C. E. Burger, Philips Tech. Rev. **11**, 291 (1950).
- ⁴⁵H. R. Splettstosser, Mater. Eval. **XXV**, 245 (1967).
- ⁴⁶H. R. Splettstosser, J. Test. Eval. **1**, 336 (1973).
- ⁴⁷K. Doi, "Wiener Spectrum Analysis of Quantum Statistical Fluctuation and Other Noise Sources in Radiography," in *Television in Diagnostic Radiology*, edited by R. D. Moseley and J. H. Rust (Aesculapius, Birmingham, AL, 1969), pp. 313-333.
- ⁴⁸R. K. Swank, J. Appl. Phys. **44**, 4199 (1973).
- ⁴⁹R. K. Swank, J. Appl. Phys. **45**, 3673 (1974).
- ⁵⁰J. C. Dainty and R. Shaw, *Image Science* (Academic, New York, 1974).
- ⁵¹K. Doi and K. Rossmann, "Measurements of Optical and Noise Properties of Screen-Film Systems in Radiography," in *Medical X-Ray Photo-Optical Systems Evaluation*, Proc. SPIE, edited by K. E. Weaver, R. F. Wagner, and D. J. Goodenough (SPIE, Palo Verdes Estates, CA, 1975), Vol. 56, pp. 45-53.
- ⁵²R. F. Wagner and K. E. Weaver, "Noise Measurements on Rare-Earth Intensifying Screen Systems," in *Medical X-Ray Photo-Optical Systems Evaluation*, Proc. SPIE, edited by K. E. Weaver, R. F. Wagner, and D. J. Goodenough (SPIE, Palo Verdes Estates, CA, 1975), Vol. 56, pp. 198-207.
- ⁵³R. F. Wagner, Med. Phys. **4**, 157 (1977).
- ⁵⁴T. R. Fewell and K. E. Weaver, "The Measurement of Diagnostic X-Ray Spectra with a High Purity Germanium Spectrometer," in *Medical X-Ray Photo-Optical Systems Evaluation*, Proc. SPIE, edited by K. E. Weaver, R. F. Wagner, and D. J. Goodenough (SPIE, Palo Verdes Estates, CA, 1975), Vol. 56, pp. 9-18.
- ⁵⁵D. J. Goodenough, K. Rossmann, and L. B. Lusted, Invest. Radiol. **8**, 339 (1973).
- ⁵⁶D. J. Goodenough, K. Rossmann, and L. B. Lusted, Radiology **110**, 89 (1974).
- ⁵⁷D. J. Goodenough and C. E. Metz, J. Acoust. Soc. Am. **55**, 111 (1974).
- ⁵⁸C. E. Metz and D. J. Goodenough, J. Nucl. Med. **14**, 873 (1973).
- ⁵⁹R. H. Morgan, Radiology **86**, 403 (1966).
- ⁶⁰F. J. Shea and M. C. Ziskin, Invest. Radiol. **7**, 147 (1972).
- ⁶¹H. L. Kundel, private communication (1972).
- ⁶²G. A. Hay, Nature **211**, 1380 (1966).
- ⁶³K. Rossmann, "Image Quality and Patient Exposure," in *Current Problems in Radiology* (Year Book Med. Publ., Chicago, 1972), Vol. II, No. 2. A paper with a similar title was presented by K. Rossmann and K. Doi at the SPSE International Conference on Image Evaluation, Toronto, Canada, July 1976, and will appear in the Proceedings to be published by SPSE. It is an interesting survey of some of the excellent analytical and clinical studies of Rossmann and Doi carried out over the last five years.
- ⁶⁴A. E. Burgess has pointed out to the writer that this preference can not be stated without qualification: There are certainly noise-limited signals in angiography.
- ⁶⁵G. C. Higgins and L. A. Jones, J. Soc. Motion Pict. Telev. Eng. **58**, 277 (1952).
- ⁶⁶O. H. Schade, J. Soc. Motion Pict. Telev. Eng. **64**, 593 (1955).
- ⁶⁷P. G. Roetling, E. A. Trabka, and R. E. Kinzly, J. Opt. Soc. Am. **58**, 342 (1968).
- ⁶⁸G. U. V. Rao, Am. J. Roentgenol. Radium Ther. Nucl. Med. **118**, 293 (1973).
- ⁶⁹R. Shaw, Proc. SPIE **70**, 359 (1975).
- ⁷⁰E. M. Granger and K. N. Cupery, Photogr. Sci. Eng. **16**, 221 (1972).
- ⁷¹E. M. Granger, thesis, Univ. Rochester (1974).
- ⁷²U. Greis and R. Rohler, Opt. Acta **17**, 515 (1970).
- ⁷³C. F. Stromeyer and B. Julesz, J. Opt. Soc. Am. **62**, 1221 (1972).
- ⁷⁴E. M. Lowry and J. J. DePalma, J. Opt. Soc. Am. **51**, 740 (1961).
- ⁷⁵T. N. Cornsweet, *Visual Perception* (Academic, New York, 1970).
- ⁷⁶D. H. Kelley, J. Opt. Soc. Am. **60**, 98 (1970). This paper contains 18 references to work on the sine-wave response of the eye.
- ⁷⁷T. L. Thourson, "Xeroradiography," in *Medical X-Ray Photo-Optical Systems Evaluation*, Proc. SPIE, edited by K. E. Weaver, R. F. Wagner, and D. J. Goodenough (SPIE, Palo Verdes Estates, CA, 1975), Vol. 56, pp. 225-235.
- ⁷⁸A. Fenster, D. Plewes, and H. E. Johns, Med. Phys. **1**, 1 (1974).
- ⁷⁹H. E. Johns, A. Fenster, and D. Plewes, Radiology **116**, 415 (1976).
- ⁸⁰E. P. Muntz, J. Lewis, T. Azzarelli, M. Welkowsky, A. L. Morsell, E. Kaegi, and G. Jacobson, "On the Characteristics of Electron Radiographic Images in Diagnostic Radiology," in *Medical X-Ray Photo-Optical Systems Evaluation*, Proc. SPIE, edited by K. E. Weaver, R. F. Wagner, and D. J. Goodenough (SPIE, Palo Verdes Estates, CA, 1975), Vol. 56, pp. 208-223.
- ⁸¹A. D. Schnitzler, J. Opt. Soc. Am. **66**, 608 (1976).
- ⁸²A. D. Schnitzler, J. Opt. Soc. Am. **66**, 617 (1976).
- ⁸³K. Rossmann, Radiology **113**, 541 (1974).
- ⁸⁴L. M. Biberman and S. Nudelman, Eds., *Photoelectronic Imaging Devices. Volume 1: Physical Processes and Methods of Analysis. Volume 2: Devices and Their Evaluation* (Plenum, New York, 1971).
- ⁸⁵L. M. Biberman, Ed., *Perception of Displayed Information* (Plenum, New York, 1973).
- ⁸⁶*Image Analysis and Evaluation*, Tech. Digest Int. Conf., Toronto, Canada, July 1976 (SPSE, Washington, DC), to be published.
- ⁸⁷*A Literature Survey on Image Quality Evaluation* (Perkin-Elmer Corp., City, 1971), ER-177. This report contains several hundred useful references, many of which are accompanied by abstracts, summaries, and/or comments.
- ⁸⁸R. Shaw, Ed., *Selected Readings in Image Evaluation* (SPSE, Washington, DC, 1976), to be published.